

## Electron-Donor Molecules

## Redox-Active Guanidines with One or Two Guanidino Groups and Their Integration in Low-Dimensional Perovskite Structures

Petra Walter,<sup>[a]</sup> Elisabeth Kaifer,<sup>[a]</sup> Hendrik Herrmann,<sup>[a]</sup> Hubert Wadepohl,<sup>[a]</sup> Olaf Hübner,<sup>[a]</sup> and Hans-Jörg Himmel<sup>\*[a]</sup>

**Abstract:** Redox-active guanidines are versatile reagents in redox and proton-coupled electron-transfer (PCET) reactions. Recently, they were integrated as sacrificial electron donors for the prohibition of metal oxidation in perovskite materials. Herein we report the synthesis and characterization of several

new redox-active guanidines with aromatic (benzene, naphthalene or anthraquinone) cores. Two of these compounds are then integrated in lead iodide materials. The structure, thermal stability and optical band-gap of the resulting materials are evaluated.

## Introduction

Redox-active organic molecules are of interest for several applications, ranging from synthetic chemistry to materials science.<sup>[1–4]</sup> Guanidino-functionalized aromatic compounds (GFAs) constitute a relatively new class of compounds developed by our group.<sup>[5,6]</sup> The redox-properties of these compounds can be tuned by the number and position of the guanidino groups attached to an aromatic core. Figure 1a shows as examples the three compounds 1,4-bis(tetramethylguanidino)-benzene (**1**),<sup>[7]</sup> 1,2,4,5-tetrakis(tetra-methylguanidino)-benzene,<sup>[8]</sup> and a hexakis-(guanidino)-benzene derivative.<sup>[9]</sup> The redox potential becomes more negative with increasing number of guanidino groups. In their oxidized state, some GFA compounds are versatile proton-coupled electron-transfer (PCET) reagents ( $2e^-$ ,  $2H^+$  transfer as shown exemplary for compound **1** in Figure 1b).<sup>[5,10–12]</sup> Reduction of the oxidized (dicationic) form is favored by the distinct Brønsted basicity<sup>[5,13,14]</sup> of the reduced state (e.g. protonated tetramethylguanidine exhibits a  $pK_a$  value of 15.2 in water and 23.3 in  $CH_3CN$ , and protonated tetramethylguanidino-benzene<sup>[15]</sup> a  $pK_a$  value of 12.2 in water and 20.6 in  $CH_3CN$ ). Further studies demonstrate a massive increase of the power to oxidize substrates even with relatively high redox potentials in the presence of strong acids.<sup>[16]</sup> Protonated redox-active guanidines could be re-oxidized by dioxygen, a reaction that is accelerated by a catalyst.<sup>[11]</sup> Hence, redox-active guanidines could be used as redox-catalyst for the oxidation of several organic substrates, with dioxygen as terminal oxidant.<sup>[11]</sup> Recently we found that

the integration of (protonated) redox-active guanidine 1,4-bis(guanidino)-benzene (**2**, Figure 2)<sup>[17]</sup> in perovskite materials is a possibility to protect the device from oxidative damage.<sup>[17]</sup> As sacrificial electron donor, twofold protonated **2** fulfills the task of capturing dioxygen diffusing into the layer by a proton-coupled electron transfer (PCET) reaction ( $2e^-$ ,  $2H^+$  transfer) in which the dioxygen is converted to water while the redox-active organic cation is oxidized.

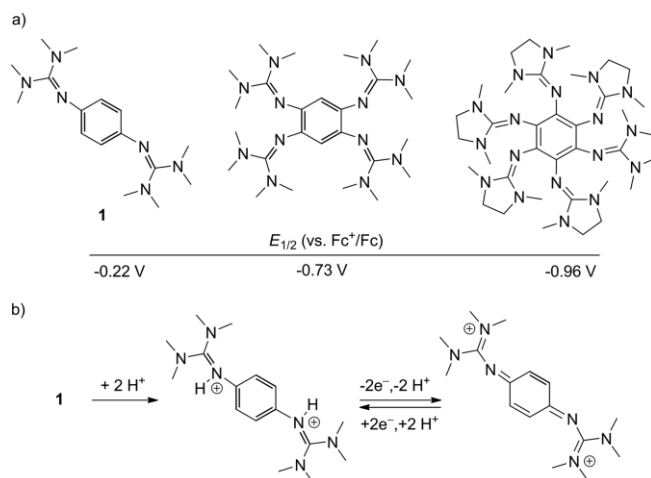


Figure 1. (a) Lewis structure of redox-active guanidines with guanidino groups attached to a benzene core. The redox potentials vs.  $Fc^+/Fc$  (in  $CH_3CN$  solution) decrease with increasing number of guanidino groups. (b) Reaction equations showing the PCET reactivity of compound **1**.

In the following, we briefly summarize some aspects of the research on perovskites to motivate the advantages of integrating redox-active organic cations. Perovskite materials are currently intensively studied as absorber and hole-transporting components in solar cell devices.<sup>[18–22]</sup> Research initially concentrated on lead perovskites of the general formula  $APbX_3$ , where A denotes a monocation and X a heavier halogen. As demonstrated already 40 years ago, the band-gap of these

[a] Anorganisch-Chemisches Institut, Ruprecht-Karls-Universität Heidelberg, Im Neuenheimer Feld 270, 69120 Heidelberg, Germany  
E-Mail: hans-jorg.himmel@aci.uni-heidelberg.de  
<http://www.uni-heidelberg.de/fakultaeten/chemgeo/aci/himmel/>

Supporting information and ORCID(s) from the author(s) for this article are available on the WWW under <https://doi.org/10.1002/ejic.201900975>.

© 2019 The Authors. Published by Wiley-VCH Verlag GmbH & Co. KGaA. This is an open access article under the terms of the Creative Commons Attribution License, which permits use, distribution and reproduction in any medium, provided the original work is properly cited.

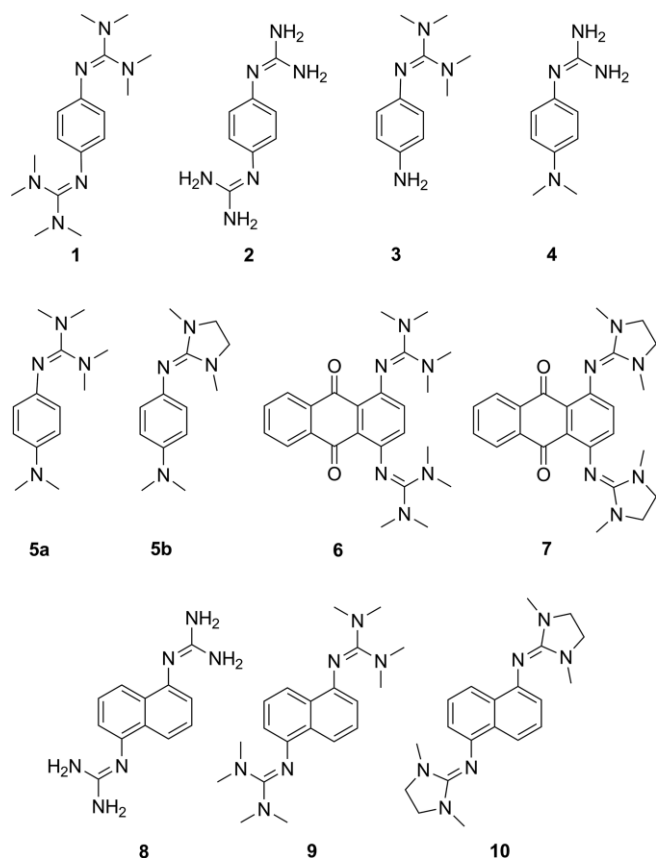


Figure 2. The redox-active bisguanidines **1** [*p*-bis(tetramethyl)guanidino-benzene] and **2** (*p*-bisguanidino-benzene) studied previously, and the new redox-active guanidines **3–10** reported herein.

compounds could be modified through the halogen (or mixtures of different halogens).<sup>[23]</sup> For a “3D perovskite” structure the choice of possible cations (A) is very much limited, and include methylammonium ( $\text{CH}_3\text{NH}_3^+$ , usually denoted MA), as well as formamidinium [ $\text{HC}(\text{NH}_2)_2^+$ , FA], guanidinium [ $\text{C}(\text{NH}_2)_3^+$ , GUA], and heavy alkali metals, e.g. caesium.

Guanidinium ions are particularly attractive due to the absence of a dipole moment that is made responsible for the large hysteresis in the current-voltage curves.<sup>[24–26]</sup> The mechanochemical synthesis of hybrid organic-inorganic guanidinium lead iodides was recently evaluated.<sup>[27]</sup> Obviously, mixtures of two of these cations were also studied. For example, the use of a perovskite  $\text{APbI}_3$ , where A is a mixture of formamidinium and methylammonium cations, leads to an enhanced short-circuit current compared with  $(\text{MA})\text{PbI}_3$ .<sup>[28]</sup> It was shown that solar cells with  $\text{Cs}_{0.2}(\text{FA})_{0.8}\text{PbI}_3$  exhibit a particularly high ambient stability (> 1000 h in the dark).<sup>[29]</sup> Very recently, dications such as ethylenediammonium ions were introduced as a third cation component together with formamidinium and methylammonium monocations in tin-lead iodides to achieve high-efficient solar cells.<sup>[30]</sup> The spectrum of materials can be further extended to low-dimensional materials, commonly denoted “2D perovskites”, “1D perovskites” or even “0D perovskites”<sup>[31–33]</sup> by integration of larger cations such as alkyl- and phenyl-substituted ammonium cations, forming e.g. layers of organic molecules interacting with each other through van-der-Waals for-

ces.<sup>[31]</sup> Organic dications such as  $\alpha,\omega$ -diammonium-alkanes were also applied.<sup>[34]</sup> If larger cations are mixed with smaller ones of comparable solubility, materials with lead iodide layers of various thickness and consequently of different material properties might result.<sup>[35,36]</sup> Some of these “2D perovskites” have been shown to exhibit an enhanced resistance to humidity.<sup>[37,38]</sup> It was also possible to modify the optical properties by the integration of cations with optically active  $\pi$ -systems.<sup>[39]</sup> Recently the search for materials in which the environmentally problematic lead is substituted by less problematic tin was intensified,<sup>[40–46]</sup> starting with the application of  $\text{CsSnI}_3$  as hole-transporting layer in solid-state dye-sensitized solar cells by Kanatzidis et al.<sup>[47]</sup> However, the application of tin-containing perovskite materials is still hampered by the inherent liability to oxidation of  $\text{Sn}^{\text{II}}$ . Several strategies were developed to circumvent this oxidation liability. Hence the addition of  $\text{SnF}_2$  was suggested, being one of the few  $\text{Sn}^{\text{II}}$  compounds that are stable towards oxidation.<sup>[48]</sup> However, the integration of fluorides is disadvantageous for the film morphology and the device properties. Moreover, the stabilizing effect of a thin coating of  $\text{SnCl}_2$  on perovskite crystallites in a  $\text{CsSnI}_3$  layer was reported.<sup>[49]</sup> In an alternative approach the tin perovskites are synthesized in a reducing atmosphere of hydrazine vapour.<sup>[50]</sup> This approach could unambiguously minimize the formation of defects during the material synthesis, but does not protect the material in the long-term from being oxidized in the device.

The integration of sacrificial organic electron donors in perovskite materials was suggested by our group as a new approach to prohibit oxidative degradation of the solar-cell devices.<sup>[17]</sup> A previous work dealt with compounds **1** and **2**. Since the hydrogen-bond donor propensities of guanidino [ $\text{NC}(\text{NH}_2)_2$ ] and amino ( $\text{NH}_2$ ) groups (with N–H functions that could form hydrogen bonds to the anions and are at the same time sterically not demanding) are essential for the integration of the redox-active guanidines in lead iodides, only compound **2** but not **1** is suitable for integration in lead iodide materials with extended lead iodide structures. On the other hand, these groups exhibit reactive N–H sites that lead to oxidative elimination and aggregation processes of the free molecules. Therefore, compounds with these groups were isolated in their protonated forms (compounds **2–4** and **8** in Figure 2), since protonation reduces their liability to oxidative degradation to an extent that makes them easy to handle. Derivatives with peralkylated guanidino and amino groups, that are less prone to oxidative degradation, were employed to study the properties (especially the redox potentials) of the un-protonated new compounds.

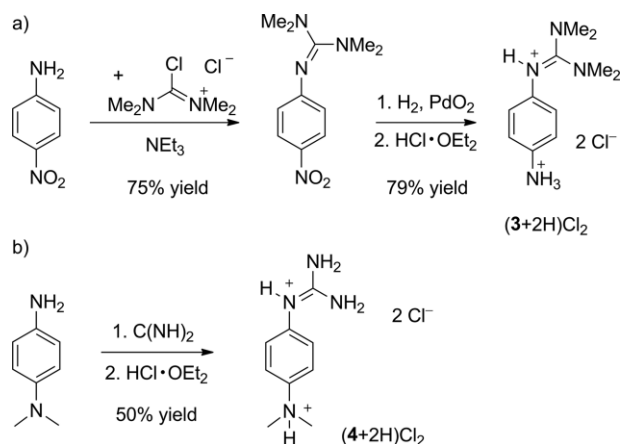
## Results and Discussion

### 1. Synthesis and Characterization

#### Compounds **3–5**

The synthesis of protonated **3** (*p*-tetramethylguanidino-aniline) started with *p*-nitroaniline (Scheme 1a). The reaction with chloro-formamidinium-chloride (obtained from tetramethylurea and oxalyl chloride) gave 1-nitro-4-tetramethylguanidino-benzene in 75 % yield (see solid-state structure in the SI). Re-

duction of this compound with dihydrogen in the presence of 3 mol-% PtO<sub>2</sub>, followed by addition of hydrochloride solution in diethyl ether, led in 79 % yield to the salt (**3**+2H)Cl<sub>2</sub>. Protonated compound **4** (*p*-guanidino-dimethylamino-benzene) was obtained by reaction of *p*-dimethylamino-aniline with cyanamide (carbodiimide) and subsequent workup with hydrochloride acid (Scheme 1b).



Scheme 1. Synthesis of the new redox-active guanidines **3** and **4** in their protonated forms, that protect them from oxidative degradation reactions.

Both compounds were crystallized as dihydrochlorides (Figure 3a). As expected, the two protons are attached to the imino N atom of the guanidino group and to the amino group. Short N–H...Cl interactions demonstrate the ability to form hydrogen-bonded networks, that is essential for the integration in stable lead iodide materials.

The redox-activity of compounds **3** and **4** is comparable to the well-known compound 1,4-bis(dimethylamino)-benzene (**2-DMAP**), that could be oxidized to “Wurster’s radical cation” and further to the dication,<sup>[51,52]</sup> and also similar to compounds **1** and **2**.<sup>[7]</sup> For compounds **3** and **4**, adiabatic first ionization energies of 5.82 and 5.88 eV were calculated (B3LYP/def2-TZVP, see SI for details). These values are close to the values of 5.36 eV calculated for **1** and 5.96 eV calculated for **2**,<sup>[7]</sup> indicating that the PCET reactivity of these compounds is comparable. Since oxidation of **3** or **4** is accompanied by further reactions due to the N–H functions, compounds **5a** and **5b** were synthesized to study the redox-activity in solution electrochemically in CV experiments. Compound **5a** is an oil, but compound **5b** is a solid at standard conditions, that was crystallized by layering a diethyl ether solution with *n*-hexane (Figure 3b). The CV curve (see Figure 4) recorded for **5a** shows two reversible oxidation waves. The first one at  $E_{\text{ox}} = -0.20$  V ( $E_{1/2} = -0.24$  V) is assigned to the redox-couple **5a**/**5a**<sup>+</sup> and the second one at  $E_{\text{ox}} = +0.06$  V ( $E_{1/2} = 0.03$  V) to **5a**<sup>+</sup>/**5a**<sup>2+</sup>. In addition, smaller and broader oxidation and reduction waves occur at higher potentials, presumably arising from protonated species readily formed in the presence of traces of water during the CV measurements. In the case of compound **5b**, the two oxidation processes ( $E_{\text{ox}} = -0.24$  V for **5b**/**5b**<sup>+</sup> and  $E_{\text{ox}} = +0.08$  V for **5a**<sup>+</sup>/**5a**<sup>2+</sup>) are not really reversible (see Figure 4) The low height of the reduction wave corresponding to the oxidation wave at  $-0.24$  V (redox-coupled **5b**<sup>+</sup>/**5b**) might result from a fast disproportionation

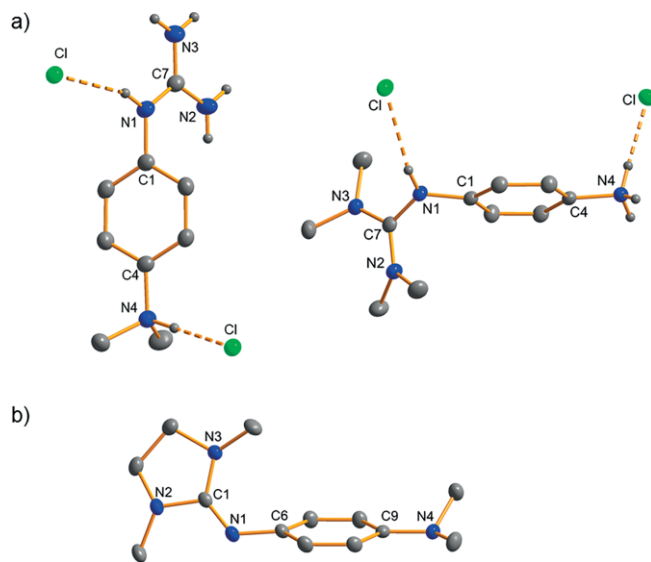


Figure 3. Illustration of the solid-state structures of (a) (**4**+2H)Cl<sub>2</sub> (left) and (**3**+2H)Cl<sub>2</sub> (right) and (b) compound **5b**. Displacement ellipsoids drawn at the 50 % probability level. Hydrogen atoms bound to carbon omitted. Selected bond lengths (in Å) for (**4**+2H)Cl<sub>2</sub>: N1–C1 1.432(2), N1–C7 1.337(2), N2–C7 1.331(2), N3–C7 1.330(2), N4–C4 1.479(2). Selected bond lengths (in Å) for (**3**+2H)Cl<sub>2</sub>: N1–C1 1.427(3), N1–C7 1.356(3), N2–C7 1.334(3), N3–C7 1.335(3), N4–C4 1.459(3). Selected bond lengths (in Å) for **5b**: N1–C1 2.282(1), N1–C6 1.406(1), N2–C1 1.386(1), N3–C1 1.390(1).

equilibrium decreasing the amount of **5b**<sup>+</sup> in the diffusion layer. For comparison, compound **1** shows a two-electron redox process (redox pair **1**/**1**<sup>2+</sup>) at a very similar potential of  $E_{1/2} = -0.22$  V in CH<sub>3</sub>CN.<sup>[7]</sup> For **2-DMAP**, one-electron oxidation to the radical monocation (“Wurster’s blue”) occurs at a potential ( $E_{1/2}$ ) of  $-0.28$  V vs. Fc<sup>+</sup>/Fc, and further one-electron oxidation to the colourless dication at  $E_{1/2} = +0.31$  V vs. Fc<sup>+</sup>/Fc.<sup>[51–53]</sup> Hence the potentials for oxidation to the radical monocation are very similar for **5a** and **2-DMAP**. On the other hand, the presence of the guanidino group in **5a** in place for the amino group in **2-DMAP** decreases significantly the potential needed for two-electron oxidation.

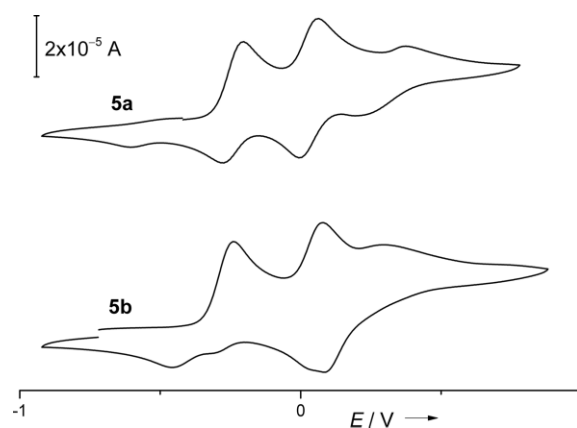


Figure 4. CV curves [CH<sub>3</sub>CN, Ag/AgCl reference electrode, 0.1 M N(*n*Bu)<sub>4</sub>(PF<sub>6</sub>) as supporting electrolyte, scan speed 100 mV s<sup>-1</sup>] for compounds **5a** and **5b** (measured in direction of oxidation). Potential values given vs. Fc/Fc<sup>+</sup>.

### Compounds 6 and 7

The synthesis of bisguanidines with anthraquinone core was accomplished in one step starting with commercially available 1,4-diamino-anthraquinone. Red-purple crystals of compound **6** were grown by diffusion of *n*-hexane into a CH<sub>3</sub>CN solution. Figure 5 illustrates the solid-state structure of **6**. Unfortunately, a 1,4-bisguanidino-anthraquinone with two NC(NH<sub>2</sub>)<sub>2</sub> groups is not accessible, at least not by following a similar protocol as for the synthesis of compound **4**. In the UV/Vis spectrum of CH<sub>3</sub>CN solutions, compound **6** shows a strong, sharp band at 254 nm and a broader one around 360 nm in the UV region. Moreover, a broad band centered at 544 nm was measured in the Vis region. TD-DFT calculations (B3LYP/def2-TZVP/COSMO, see SI for details) on **6** found the lowest-energy transition at 558 nm, in pleasing agreement with the experiments. Similarly, the UV/Vis spectra of solutions of compound **7** in CH<sub>3</sub>CN exhibit bands due to molecular electronic transitions at 252, 349 and 536 nm. Figure 6 displays the CV curves of compounds **6** and **7**. Compound **6** is oxidized at  $E_{\text{ox}} = +0.07$  V and reduced back to the neutral molecule at  $E_{\text{red}} = +0.01$  V vs. Fc/Fc<sup>+</sup> ( $E_{1/2} = +0.04$  V). These redox-processes are assigned to the redox-couple **6**/**6**<sup>2+</sup>. On the other hand, for **7** two one-electron oxidation waves (at  $E_{\text{ox}} = -0.01$  and  $+0.12$  V) were measured (Figure 6), as well as two one-electron reduction waves (at  $E_{\text{red}} = -0.08$  and  $+0.05$  V vs. Fc/Fc<sup>+</sup>), resulting in  $E_{1/2}$  values of  $-0.06$  V for the redox couple **7**<sup>+/</sup>/**7** and  $+0.09$  V for **7**<sup>2+/</sup>/**7**<sup>+</sup>. Both redox processes are reversible.

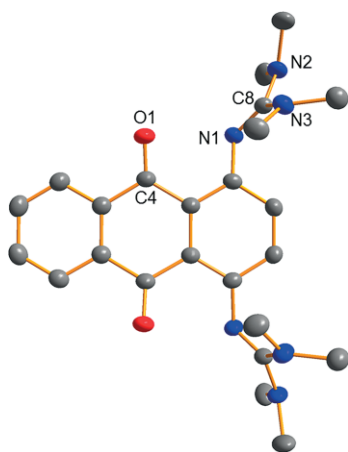


Figure 5. Illustration of the solid-state structure of compound **6**. Displacement ellipsoids drawn at the 50 % probability level. Hydrogen atoms omitted. Selected bond lengths (in Å): N1–C8 1.2947(17), N2–C8 1.3789(17), N3–C8 1.3817(17), O1–C4 1.2236(17).

Protonation of red-purple **6** with two equivalents of NH<sub>4</sub>PF<sub>6</sub> led to the orange salt (**6**+2H)(PF<sub>6</sub>)<sub>2</sub> (Scheme 2). In the UV/Vis spectra, the lowest-energy band of **6** centered at 544 nm shifted to 456 nm (3548 cm<sup>-1</sup> shift) upon protonation (Figure 7). This large hypsochromic shift could be rationalized by the interactions between the N–H protons and the two carbonyl oxygen atoms. In this context it is worth mentioning that hypsochromic shifts upon protonation of not-redox-active mono-guanidine compounds, including guanidino-benzene, and the influence of intermolecular hydrogen-bonding to anions were recently analysed.<sup>[54]</sup> A similar hypsochromic shift was observed upon pro-

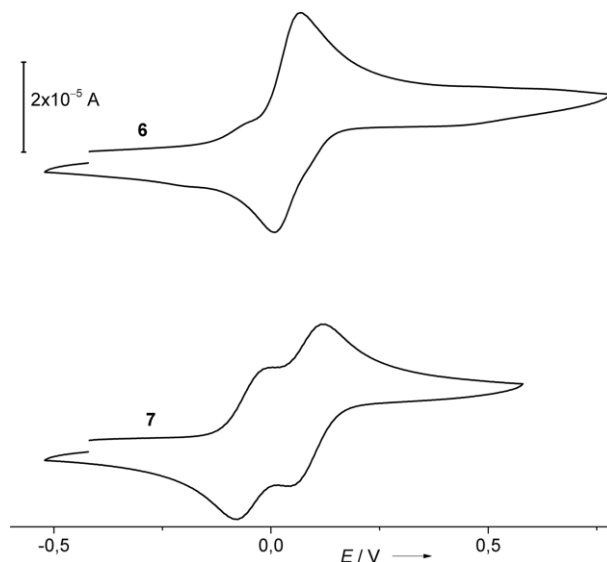
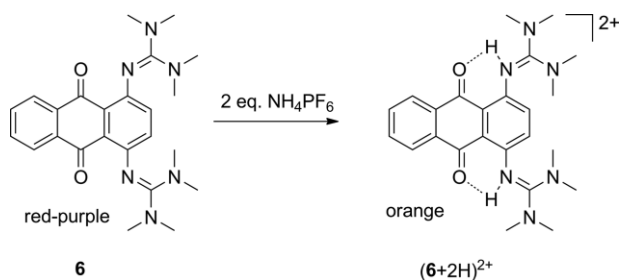


Figure 6. CV curves [CH<sub>3</sub>CN, Ag/AgCl reference electrode, 0.1 M N(*n*Bu)<sub>4</sub>(PF<sub>6</sub>) as supporting electrolyte, scan speed 100 mV s<sup>-1</sup>] for compounds **6** and **7** (measured in direction of oxidation). Potential values given vs. Fc/Fc<sup>+</sup>.



Scheme 2. Protonation of red-purple **6** leading to orange (**6**+2H)(PF<sub>6</sub>)<sub>2</sub>.

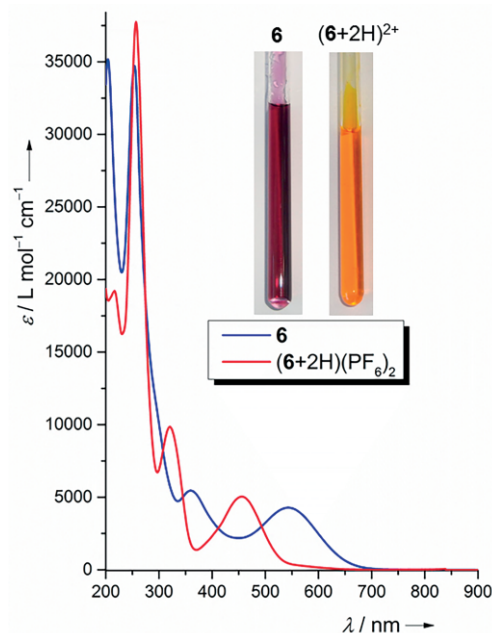


Figure 7. Electronic absorption spectra (in CH<sub>3</sub>CN) for **6** and (**6**+2H)(PF<sub>6</sub>)<sub>2</sub>. The inset shows photos of NMR tubes containing CH<sub>3</sub>CN solutions of the two compounds.

tonation of **7** [from  $\lambda_{\max} = 536$  nm for **7** to  $\lambda_{\max} = 462$  nm for  $(\mathbf{7}+2\text{H})(\text{PF}_6)_2$ ]. Figure 8 illustrates the solid-state structures of the protonated compounds.

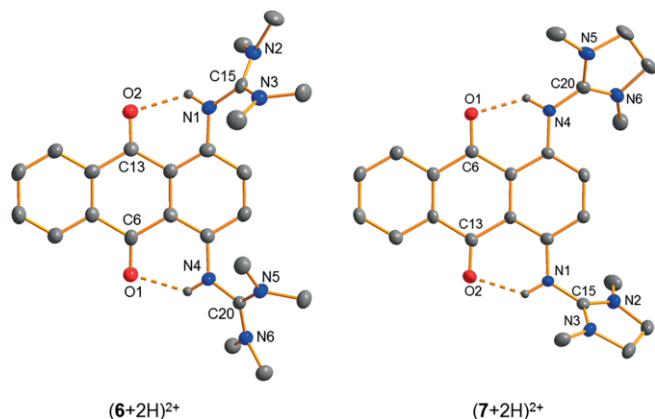
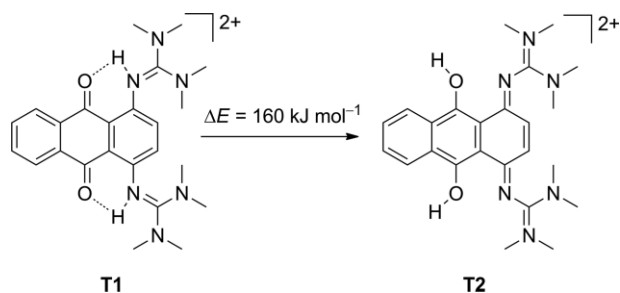


Figure 8. Illustration of the solid-state structures of  $(\mathbf{6}+2\text{H})^{2+}$  and  $(\mathbf{7}+2\text{H})^{2+}$ . Displacement ellipsoids drawn at the 50 % probability level. C–H hydrogen atoms omitted. Selected bond lengths (in Å) for  $(\mathbf{6}+2\text{H})^{2+}/(\mathbf{7}+2\text{H})^{2+}$ : N1–C15 1.361(4)/1.364(4), N2–C15 1.324(4)/1.321(4), N3–C15 1.337(4)/1.328(3), N4–C20 1.352(4)/1.363(3), N5–C20 1.332(4)/1.329(4), N6–C20 1.336(4)/1.324(4), O1–C6 1.231(3)/1.235(3), O2–C13 1.247(3) /1.243(3).

Quantum-chemical calculations (B3LYP/def2-TZVP, see SI for details) found two tautomeric structures for  $(\mathbf{6}+2\text{H})^{2+}$ . A structure close to the experimental solid-state structure defines the global-energy minimum structure (**T1**). It exhibits two asymmetric N–H...O bridges. In the second tautomer (**T2**, Scheme 3) the protons are attached to the oxygen atoms. Consequently, tautomerization from **T1** to **T2** is accompanied by reduction of the quinone to the dihydroquinone and oxidation of the outer ring with the two guanidino groups. The aromaticity in the  $\text{C}_6$  ring with the two guanidino groups is removed and instead the central ring is now participating in the aromaticity (see Lewis representation in Scheme 3). Isomer **T2** exhibits a significantly higher energy [ $\Delta E = 160$  kJ mol<sup>-1</sup> (1.66 eV)] according to B3LYP/def2-TZVP, see SI for details], in line with the experimental results.



Scheme 3. Lewis representations of the two calculated tautomers of  $(\mathbf{6}+2\text{H})^{2+}$  and their relative energies (according to B3LYP/def2-TZVP, see SI for details).

TD-DFT calculations (B3LYP/def2-TZVP/COSMO) were carried out to gain further information about the electronic transitions. In pleasing agreement with the experimental results ( $\lambda_{\max} = 456$  nm), the lowest-energy transition was predicted at  $\lambda = 476$  nm. The blue-shift upon protonation of 3063 cm<sup>-1</sup> calculated for the isolated dication compares with the experimental

blue-shift of 3548 cm<sup>-1</sup> for the dication in solution. Furthermore, the calculations show that the lowest-energy transition results from an excitation of an electron from the HOMO into the LUMO. Figure 9 illustrates the shapes of the HOMO and LUMO for **6** and  $(\mathbf{6}+2\text{H})^{2+}$ , from which one can see that the excitation has charge-transfer character from the electron-rich ring with the two guanidino groups to the electron-poor quinone ring. For the second energetically disfavored tautomer **T2**, the calculations found a relatively intense lowest-energy transition at 541 nm, which does not fit to the experimental results. Hence both experiment and theory indicate that  $(\mathbf{6}+2\text{H})^{2+}$  exists exclusively in its lowest-energy tautomeric form, **T1**. Further experiments showed that it was not possible to photo-tautomerize the compound.

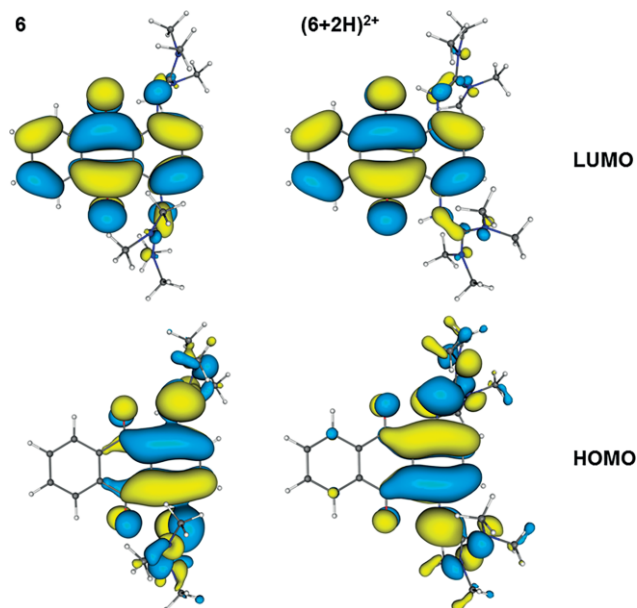
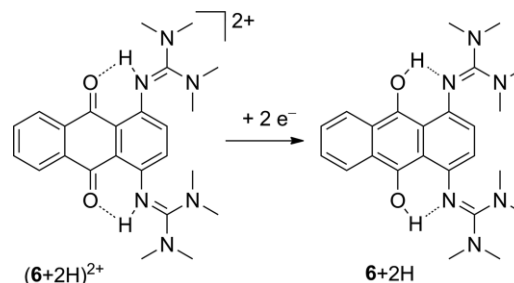


Figure 9. Illustration of the isodensity surfaces for the HOMO and LUMO in **6** and in  $(\mathbf{6}+2\text{H})^{2+}$  (from B3LYP/def2-TZVP/COSMO calculations).

The CV curves indicate that reversible two-electron reduction of the protonated compounds  $(\mathbf{6}+2\text{H})(\text{PF}_6)_2$  and  $(\mathbf{7}+2\text{H})(\text{PF}_6)_2$  is possible (see SI for more information). For  $(\mathbf{6}+2\text{H})(\text{PF}_6)_2$ , one obtains  $E_{\text{red}} = -0.88$  V and  $E_{\text{ox}} = -0.84$  V. For  $(\mathbf{7}+2\text{H})(\text{PF}_6)_2$ , values of  $E_{\text{red}} = -0.78$  V and  $E_{\text{ox}} = -0.73$  V vs.  $\text{Fc}^+/\text{Fc}$  were measured. As shown in Scheme 4, two-electron reduction should be accompanied by transfer of the protons from the guanidino groups to the oxygen atoms and formation of an electron-rich



Scheme 4. Two-electron reduction of  $(\mathbf{6}+2\text{H})^{2+}$  to give the electron-rich dihydro-antraquinone derivative **6+2H**.

dihydro-anthraquinone. The results of quantum-chemical calculations on the reduced form **6**+2H support such an electronic structure and also confirm the formation of intramolecular O–H...N interactions (see SI).

### Compounds **8**–**10**

The synthesis started for all three compounds with 1,5-diaminonaphthalene-dihydrochloride. Reaction with chloroformamidinium-chloride yielded **9**, and reaction with 2-chloro-1,3-dimethyl-4,5-dihydro-1*H*-imidazolium chloride yielded **10**. Compounds **9** and **10** were crystallized from *n*-hexane and acetonitrile solutions, respectively, and Figure 10 illustrates their solid-state structures.

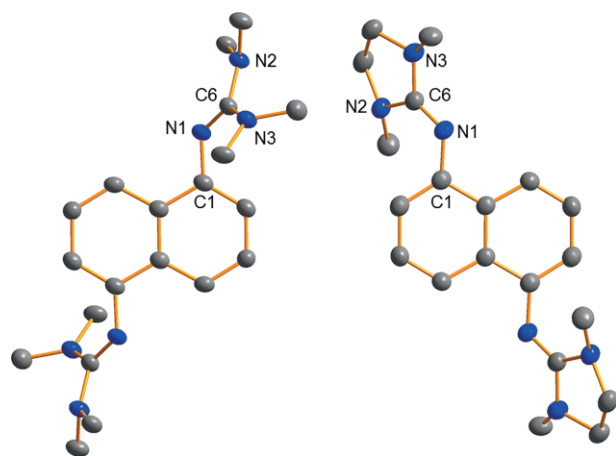


Figure 10. Illustration of the solid-state structures of **9** (left) and **10** (right). Displacement ellipsoids drawn at the 50 % probability level. Hydrogen atoms omitted. Selected bond lengths (in Å) for **9**: N1–C1 1.407(3), N1–C6 1.298(2), N2–C6 1.377(3), N3–C6 1.385(3). Selected bond lengths (in Å) for **10**: N1–C1 1.392(5), N1–C6 1.293(5), N2–C6 1.386(5), N3–C6 1.383(5).

The CV curves of **9** and **10** show non-reversible oxidation waves at  $E_{\text{ox}} = +0.43$  V vs. Fc/Fc<sup>+</sup> for **9** and  $E_{\text{ox}} = +0.07$  V vs. Fc/Fc<sup>+</sup> for **10** (Figure 11). The reason for the non-reversibility is

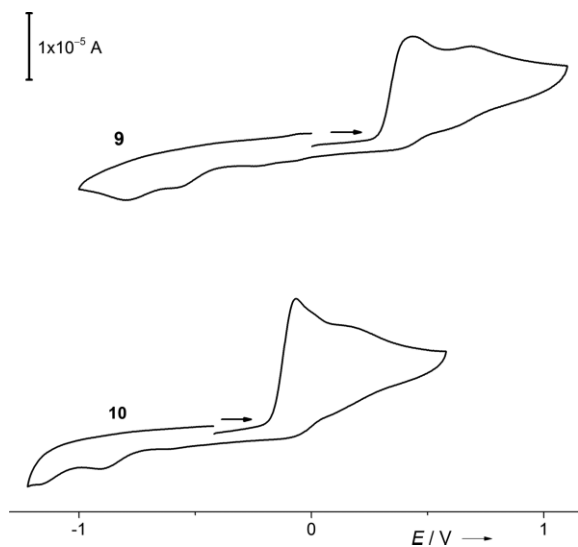


Figure 11. CV curves [ $\text{CH}_3\text{CN}$ , Ag/AgCl reference electrode, 0.1 M  $\text{N}(\text{nBu})_4(\text{PF}_6)$ ] as supporting electrolyte, scan speed  $100 \text{ mV s}^{-1}$ ] for compounds **9** and **10** showing irreversible oxidation waves. Potential values given vs. Fc/Fc<sup>+</sup>.

not fully clear, but the positions 4 and 8 of the naphthalene core *para* to the guanidino groups are activated and prone to C–C self-coupling reactions to give tetrakisguanidino-binaphthyl derivatives. Since such reactions are outside the scope of this work, they were not further pursued.

Finally, the salt  $(\mathbf{8}+2\text{H})\text{Cl}_2$  was obtained directly by reaction of 1,5-diaminonaphthalene-dihydrochloride with cyanamide (carbodiimide). Its solid-state structure is illustrated in Figure 12. As expected, the two imino-N atoms of each guanidino group are protonated, and the structure shows N–H...Cl hydrogen bonding. The compound  $(\mathbf{9}+2\text{H})(\text{PF}_6)_2$  was prepared from **9** and two equivalents of  $\text{NH}_4\text{PF}_6$  (see also Figure 12). Again, protonation occurred exclusively at the imino N atoms of the guanidino groups and hydrogen-bond interactions to the anions were established.

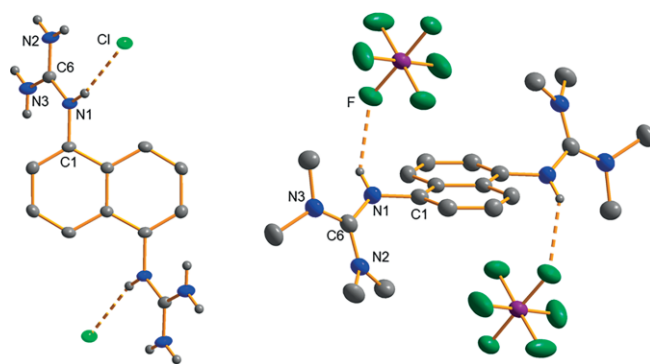


Figure 12. Illustration of the solid-state structures of  $(\mathbf{8}+2\text{H})\text{Cl}_2$  (left) and  $(\mathbf{9}+2\text{H})(\text{PF}_6)_2$  (right). Displacement ellipsoids drawn at the 50 % probability level. Hydrogen atoms bound to carbon omitted. Selected bond lengths (in Å) for  $(\mathbf{8}+2\text{H})\text{Cl}_2$ : N1–C1 1.4241(18), N1–C6 1.3370(19), N2–C6 1.329(2), N3–C6 1.327(2). Selected bond lengths (in Å) for  $(\mathbf{9}+2\text{H})(\text{PF}_6)_2$ : N1–C1 1.427(3), N1–C6 1.354(3), N2–C6 1.336(3), N3–C6 1.328(3).

## 2. Integration of Redox-Active Guanidines in Lead Iodides

Reactions were carried out with compounds **3**, **4** and **8** (applied in their twofold-protonated form). While no clean product could be isolated in the reactions with compound **8**, new organic-inorganic hybrid materials were obtained by reacting the protonated organic electron-donors **3** and **4** with lead iodide in aqueous HI solutions. In the reactions, the corresponding hydrochloride  $(\mathbf{3}+2\text{H})\text{Cl}_2$  resp.  $(\mathbf{4}+2\text{H})\text{Cl}_2$  was first dissolved in a small amount of concentrated HI (57 % in water) to replace the counterions (chloride → iodide). Then a second solution containing  $\text{PbI}_2$  in concentrated HI, heated to a temperature of 75 °C, was added. During re-cooling of the mixture to room-temperature a microcrystalline precipitate of the raw-product formed, that was isolated, washed twice with MeOH and dried under vacuum. Finally, the raw-product was re-dissolved in concentrated HI at a temperature of 60 °C, some EtOH added and the solution cooled back to room temperature. In the case of the reactions with  $(\mathbf{3}+2\text{H})\text{Cl}_2$ , crystals of the product suitable for structural characterization with single-crystal X-ray diffraction were obtained during re-cooling to room-temperature, and the product,  $(\mathbf{3}+2\text{H})\text{Pb}_2\text{I}_6$ , was isolated in 90 % yield. In the case of  $(\mathbf{4}+2\text{H})\text{Cl}_2$ , crystals of the product were obtained at low tem-

peratures (5 °C). These crystals were washed with pentane and hexane, and subsequently dried under vacuum to give the product,  $(4+2H)PbI_4$ , in 70 % yield. Figure 13 and Figure 14 display the structures of the two new materials. In both cases lead iodide chains are formed, composed of  $PbI_6$  octahedra that share some of their edges with neighboring octahedra. In  $(3+2H)Pb_2I_6$ , each octahedron is connected to five neighboring octahedra. Hence, it shares five out of twelve edges with adjacent octahedra, leading to a double-chain type structure highlighted in Figure 13b. By contrast, each octahedron in  $(4+2H)PbI_4$  is connected only to two neighboring octahedra, as

shown in Figure 14b. The guanidine substituents are aligned along the chains. In  $(3+2H)Pb_2I_6$ , each  $(3+2H)^{2+}$  unit establishes four short  $N-H\cdots I$  interactions with the lead iodide chains (Figure 13c). In  $(4+2H)PbI_4$ , three short  $N-H\cdots I$  interactions between each  $(4+2H)^{2+}$  unit and the lead iodide chains were found (Figure 14c).

The volume of the unit cells also differ. For  $(3+2H)Pb_2I_6$  (monoclinic, space group  $C2/c$ ), a volume of  $V = 5222.9(3) \text{ \AA}^3$  was derived. In the case of  $(4+2H)PbI_4$  (monoclinic, space group  $P2_1/c$ ), the volume is considerably smaller [ $V = 1906.73(2) \text{ \AA}^3$ ]. In this context it should be added that recently 2D layer struc-

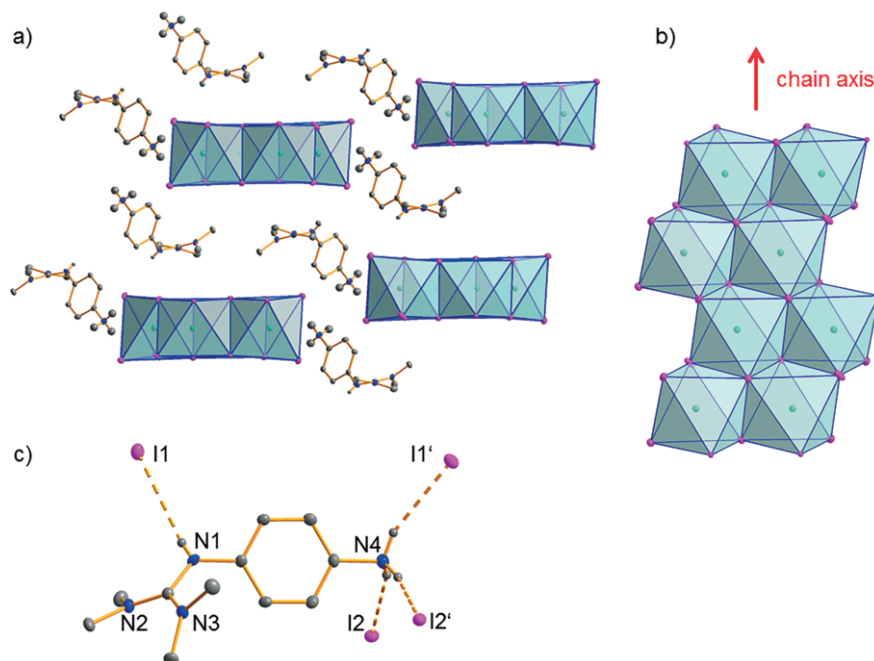


Figure 13. (a) Illustration of the structure of  $(3+2H)Pb_2I_6$  in the crystalline compound from two perspectives (view in the direction of the chains). (b) Perpendicular view on a segment of one chain highlighting the connectivity of the octahedral units through shared edges. (c) View on one redox-active dication highlighting its interactions via  $N-H\cdots I$  contacts. C-H hydrogen atoms omitted. Vibrational ellipsoids drawn at the 50 % probability level.

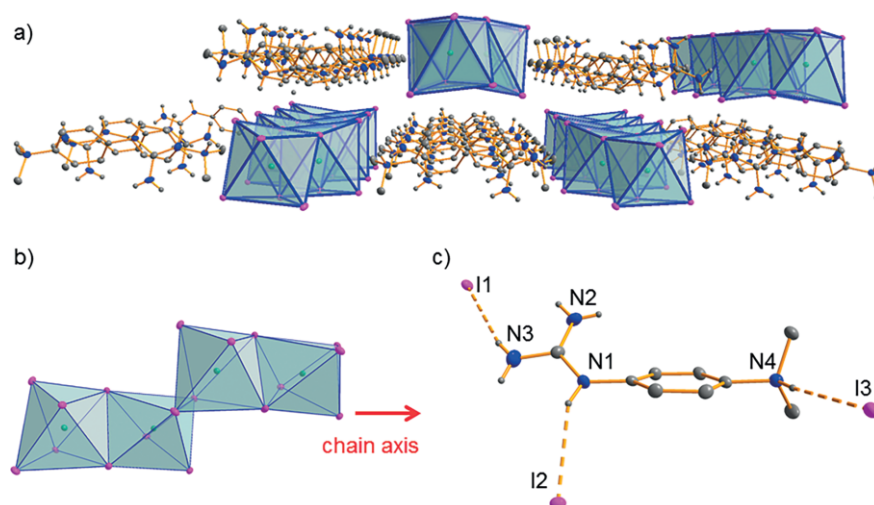


Figure 14. (a) Illustration of the structure of  $(4+2H)PbI_4$  in the crystalline compound from two perspectives (view in the direction of the chains). (b) Perpendicular view on a segment of one chain highlighting the connectivity of the octahedral units through shared edges. (c) View on one redox-active dication highlighting its interactions via  $N-H\cdots I$  contacts. C-H hydrogen atoms omitted. Vibrational ellipsoids drawn at the 50 % probability level.

tures were obtained with twofold protonated *p*-dimethylamino-aniline.<sup>[55]</sup> By contrast, 1D chain structures were obtained with twofold protonated *p*-amino-aniline.

Electronic excitation spectra of the materials (3+2H)Pb<sub>2</sub>I<sub>6</sub> and (4+2H)PbI<sub>4</sub> were collected as diffuse reflection measurements for the materials embedded in a BaSO<sub>4</sub> matrix (Figure 15a). The spectrum recorded for (3+2H)Pb<sub>2</sub>I<sub>6</sub> shows an edge-type structure with an onset of absorption at ca. 450 nm, and a maximum of absorption at around 400 nm. For (4+2H)PbI<sub>4</sub>, a similar onset of the absorption, but a slight blue-shift of the maximum of the sharp absorption to ca. 390 nm was measured (Figure 15a). By using the direct band gap Tauc plot (Figure 15b), optical band gaps of ca. 2.75 eV were deduced.<sup>[56]</sup> For comparison, in a series of lead iodide, bromide and chloride 2D perovskites with acene alkylammonium cations optical band gaps (estimated with the direct band gap Tauc formalism) between 2.7–4.5 eV were determined.<sup>[57]</sup> For (2+2H)Pb<sub>2</sub>I<sub>6</sub> and (3+2H)Sn<sub>2</sub>I<sub>6</sub>, optical band gaps of 2.81 eV and 2.85 eV were derived.<sup>[17]</sup>

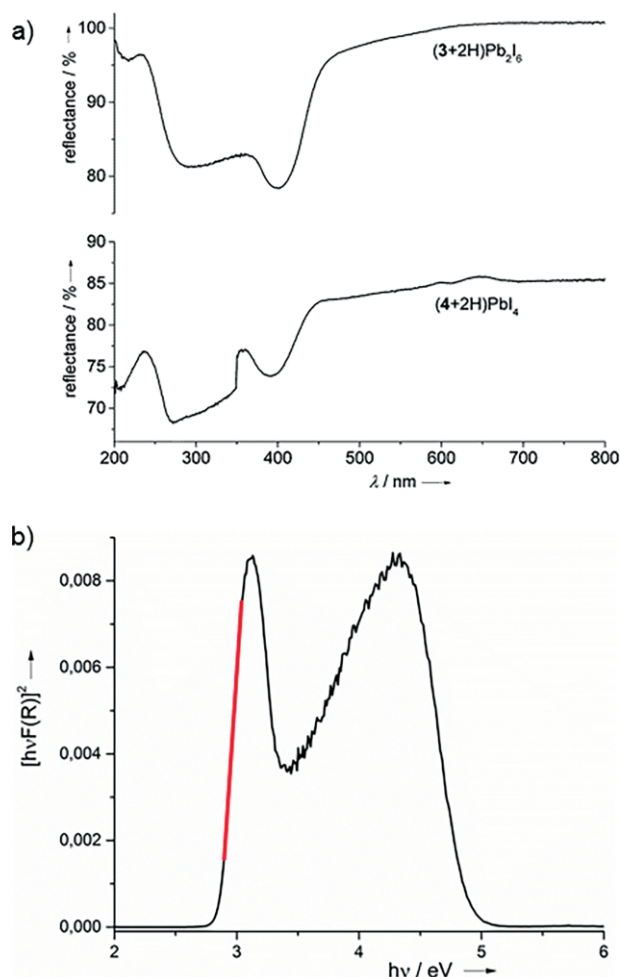


Figure 15. (a) Electron spectra (diffuse reflectance of the material in a BaSO<sub>4</sub> matrix) of (3+2H)Pb<sub>2</sub>I<sub>6</sub> and (4+2H)PbI<sub>4</sub>. (b) Tauc plot for (3+2H)Pb<sub>2</sub>I<sub>6</sub> and linear fit (red line) for estimation of the optical band-gap.

Dynamic difference calorimetry (DSC) measurements for (3+2H)Pb<sub>2</sub>I<sub>6</sub> under inert-gas atmosphere found evidence for a sharp endothermic peak around 286 °C (Figure 16) that is assigned to the melting process. The enthalpy change for this

endothermic process is 33.1 J g<sup>-1</sup>. At higher temperatures decomposition commences, with a sharp exothermic decomposition peak at ca. 311 °C (exothermic process with an enthalpy change of 15.4 J g<sup>-1</sup>). These results clearly show that the thermal stability of the material is sufficiently high.<sup>[58]</sup> For (4+2H)PbI<sub>4</sub>, a broader endothermic signal around 221 °C can be assigned to the melting process. The decomposition starts at temperatures above 270 °C. The quite large difference between the melting and decomposition temperature might be interesting for applications. Hence, perovskites with relatively low melting point, lower than the decomposition temperature, are attractive for melt processing.<sup>[59,60]</sup>

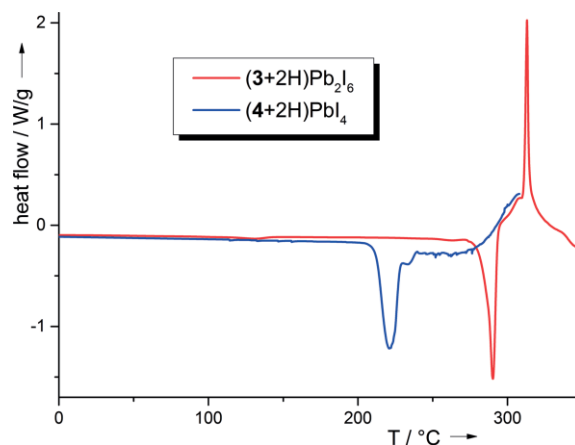


Figure 16. Differential scanning calorimetry (DSC) curves for (3+2H)Pb<sub>2</sub>I<sub>6</sub> and (4+2H)PbI<sub>4</sub>, measured under N<sub>2</sub> atmosphere with a heating rate of 15 K min<sup>-1</sup>.

Finally, high-temperature powder XRD measurements were carried out for (3+2H)Pb<sub>2</sub>I<sub>6</sub> in the presence of air (diffractograms are included in the SI). These measurements showed no changes of the material up to a temperature of 240 °C. At 242 °C the peaks decreased and at 250 °C all diffraction peaks vanished. At much higher temperatures of 420 °C and more, peaks due to mixed lead oxides appeared (see diffractograms in the SI). Hence, these measurements confirm a high thermal stability of the material, even upon exposure to air. This stability in part arises from the ability of the redox-active guanidine cations to capture the dioxygen diffusing into the material via a proton-coupled electron-transfer (PCET) reaction with dioxygen. Thereby metal oxidation (Pb<sup>II</sup> → Pb<sup>IV</sup>) is prohibited, as shown previously for materials with compound **2**<sup>[17]</sup> exhibiting a similar redox potential and pK<sub>a</sub> value and therefore similar PCET reactivity.

## Conclusions

Several new redox-active guanidines with benzene, anthraquinone and binaphthyl cores were synthesized and characterized. Their redox-properties were analyzed by CV measurements. These new compounds enrich the class of redox-active guanidines, that exhibits manifold applications, e.g. as electron donors and reagents in proton-coupled electron-transfer (PCET) reactions.<sup>[5,10]</sup> Two of the new compounds were then integrated in lead iodide materials. In addition to their role in establishing

a hydrogen-bond network that stabilizes the material, the redox-active guanidines could act as sacrificial electron donors to protect the metal ions from being oxidized by dioxygen (by PCET with dioxygen), explaining their high thermal stability even in air. The materials were structurally characterized, and their thermal stability and optical band-gaps evaluated. Both materials exhibit chains of lead iodides composed of  $\text{PbI}_6$  octahedra that share some of their edges with adjacent octahedra, but nevertheless differ in their structure. The optical band gaps of 2.75 eV derived for the materials are in a typical region for low-dimensional perovskite materials. The compounds are thermally stable up to more than 200 °C under air. In ongoing work we are studying the performance of the new redox-active guanidines in proton-coupled electron-transfer (PCET) reactions.<sup>[4]</sup> Current work on low-dimensional perovskite structures with integrated redox-active guanidines aims at the synthesis of 2D-materials with lower optical band gaps.

## Experimental Section

All synthetic work was carried out under argon atmosphere using the Schlenk technique. The starting reagents  $\text{PbI}_2$  (99 %), cyanamide (99 %), oxalyl chloride (98 %), 1,5-diamino-naphthalene (97 %) and *N,N*-dimethyl-*p*-phenylene-diamine-dihydrochloride (99 %) were obtained from Sigma Aldrich, HI (57 % in  $\text{H}_2\text{O}$ ) and *p*-nitroaniline (99 %) from Acros Organics and 1,4-diamino-anthraquinone (90 %) from abcr GmbH. All solvents were dried with an MBRAUN MB-SPS-800 solvent purification system, degassed by three freeze-pump-thaw cycles and stored over molecular sieves. IR spectra were collected on a BIORAD Excalibur FTS 3000. The acquisition of diffuse reflectance spectra was done on an Agilent Cary 5000 spectrophotometer with  $\text{BaSO}_4$  pellets of the powder materials. Elemental analysis was carried out at the Microanalytical laboratory of the chemical institutes at the Heidelberg University. Powder X-ray diffraction data were recorded with a Stoe Stadi P [ $\text{Cu-K}_\alpha$  radiation,  $\lambda = 1.5406 \text{ \AA}$ , Ge(111)-monochromated] in sealed glass capillaries as sample containers ( $\varnothing = 0.5 \text{ mm}$ ). High-temperature powder X-ray diffraction was carried out with a graphite heater element in quartz capillaries ( $\varnothing = 0.5 \text{ mm}$ ). A Cary 5000 spectrophotometer was used for diffuse reflectance measurements on  $\text{BaSO}_4$  pellets of the lead iodate materials.  $^1\text{H}$  NMR spectra were recorded on a BRUKER Avance DPX 200 machine, and  $^{13}\text{C}$  NMR spectra on a BRUKER Avance II 400maschine. Solvent resonances were taken as references for all  $^1\text{H}$  NMR spectra. A Discovery DSC 250 from TA Instruments was used for the DSC measurements. The samples were sealed in aluminum pans with lids from TA Instruments. The heating rate was set to 15 K/min. Cyclic voltammetry (CV) measurements relied on a Metrohm Autolab potentiostat PGSTAT204. The compounds were dissolved in  $\text{CH}_3\text{CN}$  ( $c = 10^{-3} \text{ mol L}^{-1}$ ), with 0.1 M  $\text{N}(\text{nBu})_4(\text{PF}_6)$  as supporting electrolyte. An Ag/AgCl electrode was used as reference electrode. The voltammograms are denoted CV curves in the text.

### **p-Tetramethylguanidinoaniline-dihydrochloride, 3-2HCl in Two Steps**

**1. Step: p-Nitro-tetramethylguanidinobenzene:** *N,N,N',N'*-Tetramethylurea (3.6 mL, 30 mmol) is dissolved in chloroform (30 mL). Then 13.0 mL (155 mmol) of oxalyl chloride is added at room temperature and the mixture heated to reflux for a period of 17 h. The solvent is removed in vacuo and the resulting residue washed twice with 20 mL portions of diethyl ether, yielding the chloroformamidinium chloride salt. This product is dissolved in acetonitrile

(20 mL). A solution of *p*-nitroaniline (2.66 g, 19.25 mmol) with triethylamine (8.4 mL, 60 mmol) in acetonitrile (30 mL) is prepared in another flask and cooled to  $-5 \text{ }^\circ\text{C}$ . At this temperature the solution of the chloroformamidinium chloride is added in portions to the nitroaniline solution. Then the solution is stirred for 5 h at 0 °C and further 16 h at room temperature. The solvent is removed in vacuo and the residue re-dissolved in aqueous HCl (5 %). After the addition of a solution of sodium hydroxide in water (40 %), the solution is extracted with diethyl ether and the organic phases are dried with  $\text{K}_2\text{CO}_3$ . The solvent is removed in vacuo, the solid residue dissolved in a small amount of acetonitrile and this solution extracted with cyclohexane. A yellow solid (3.43 g, 75 %) is obtained after solvent removal in vacuo. Crystals suitable for structural analysis by single-crystal X-ray diffraction are grown from a toluene solution.  $^1\text{H}$  NMR (199.87 MHz,  $\text{CD}_3\text{CN}$ ):  $\delta = 8.04\text{--}7.96$  (m, 2 H,  $\text{CH}_{\text{arom}}$ ), 6.67–6.59 (m, 2 H,  $\text{CH}_{\text{arom}}$ ), 2.72 (s, 12 H,  $\text{CH}_3$ ) ppm; elemental analysis (%) for  $\text{C}_{11}\text{H}_{16}\text{N}_4\text{O}_2$  ( $236.27 \text{ g mol}^{-1}$ ): calcd. C 55.92, H 6.83, N 23.71; found C 56.22, H 6.89, N 23.63.

**2. Step: p-Tetramethyl-guanidinoaniline Hydrochloride:** In a 2-L flask, *p*-nitro-tetramethylguanidinobenzene (1.18 g, 5 mmol) and PtO<sub>2</sub> (34 mg, 0.16 mmol) are suspended in 100 mL of ethyl acetate. The reaction mixture is degassed by three pump-thaw-freeze cycles. Then the mixture is frozen again and the flask evacuated. The flask is filled with an atmosphere of dihydrogen. The mixture is warmed to room temperature and stirred for a period of 20 h. During this period, the pressure decreases arising from the consumption of dihydrogen is compensated from time-to-time. The catalyst is removed by filtration through celite and to the colorless filtrate HCl in diethyl ether (15 mL, 2 M) is added. The precipitate is washed with ethyl acetate ( $2 \times 30 \text{ mL}$ ) and dried under vacuum. One obtains *p*-tetramethylguanidinoaniline-dihydrochloride as a colorless solid in a yield of 1.26 g (4 mmol, 79 %). Crystals suitable for an XRD analysis were obtained from glacial acetic acid solutions.  $^1\text{H}$  NMR (199.87 MHz,  $\text{CD}_3\text{OD}$ ):  $\delta = 7.06\text{--}6.95$  (m, 2 H, CH), 2.97 (s, 12 H,  $\text{CH}_3$ ) ppm; elemental analysis (%) for  $\text{C}_{11}\text{H}_{18}\text{N}_4 \cdot 2\text{HCl}$  ( $279.1 \text{ g mol}^{-1}$ ): calcd. C 47.32, H 7.22, N 20.07; found C 46.73, H 7.28, N 19.59; ESI+:  $m/z = 207.1758$  [ $\text{MH} + \text{-2HCl}$ ].

***N,N*-Dimethyl-*p*-guanidinoaniline Hydrochloride (4-2HCl):** *N,N*-Dimethyl-*p*-phenylenediamine dihydrochloride (4.176 g, 20 mmol) and carbodiimide (1.264 g, 30 mmol) are heated to reflux in absolute ethanol (50 mL) for a period of 30 h. The solution is cooled to room temperature and then HCl in diethyl ether (10 mL, 2M) is added. The solvent is removed in vacuo and the residual is washed with ethanol (20 mL) and diethyl ether ( $2 \times 20 \text{ mL}$ ). A colorless solid is obtained (2.8 g, 10 mmol) in a yield of 50 %. Crystals suitable for an XRD analysis were obtained from a solution in glacial acetic acid.  $^1\text{H}$  NMR (199.87 MHz,  $\text{CD}_3\text{OD}$ ):  $\delta = 7.56\text{--}7.39$  (m, 4 H,  $\text{CH}_{\text{arom}}$ ), 3.23 (s, 6 H,  $\text{CH}_3$ ) ppm; elemental analysis (%) for  $\text{C}_9\text{H}_{14}\text{N}_4 \cdot 2\text{HCl}$  ( $251.12 \text{ g mol}^{-1}$ ): calcd. C 43.04, H 6.42, N 22.31; found C 42.01, H 6.35, N 21.34; ESI+:  $m/z = 179.1325$  [ $\text{MH}^+ \cdot 2\text{HCl}$ ].

**(3+2H)Pb<sub>2</sub>I<sub>6</sub>:** A solution of *p*-tetramethylguanidinoaniline hydrochloride (0.110 g, 0.40 mmol) in aqueous HI (57 %, 5 mL) is prepared and added to a solution of lead(II)iodide (0.18 g, 0.40 mmol) in aqueous HI (57 %, 5 mL) at a temperature of 75 °C and stirred for 15 min. Then the clear yellow solution is cooled to room temperature. During this time a fine crystalline precipitate forms. The solvent is removed by filtration and the precipitate is washed twice with methanol and dried under vacuum. One obtains (3+2H)Pb<sub>2</sub>I<sub>6</sub> as a pale yellow solid (0.25 g, 0.18 mmol) with a yield of 90 % with respect to lead(II)iodide. Crystals suitable for a structural characterization by single-crystal X-ray diffraction are obtained by dissolving the product in hot aqueous HI (57 %, 4 mL) after addition

of 1 mL of ethanol. Elemental analysis (%) for  $C_{11}H_{20}N_4Pb_2I_6$  (1382.11 g mol<sup>-1</sup>): calcd. C 9.54, H 1.46, N 4.05; found C 9.57, H 1.53, N 3.99.

**(4+2H)PbI<sub>4</sub>**: A solution of *N,N*-dimethyl-*p*-guanidinoaniline hydrochloride (0.105 g, 0.40 mmol) in aqueous HI (57 %, 5 mL) is heated to 75 °C. At this temperature a solution of lead(II)iodide (0.18 g, 0.40 mmol) in aqueous HI (57 %, 5 mL) is added and the reaction mixture stirred for 1 h. The solution is cooled back to room temperature, and the clear solution is layered with ethanol and stored at 5 °C. The solution is decanted from the precipitated crystals (suitable for X-ray diffraction) which are washed with *n*-pentanol and hexane and dried subsequently under vacuum. The product **(4+2H)PbI<sub>4</sub>** is obtained as a pale yellow solid (0.26 g, 0.29 mmol) in a yield of 72 %. Elemental analysis (%) for  $C_9H_{16}N_4PbI_4$  (899.10 g mol<sup>-1</sup>): calcd. C 12.02, H 2.24, N 6.23; found C 11.93, H 1.79, N 6.45.

***N,N'*-Tetramethylguanidino-*N''*,*N'''*-dimethyl-*p*-phenylenediamine (5a)**: *N,N,N',N''*-Tetramethylurea (3.0 mL, 25 mmol) is dissolved in chloroform (35 mL). Then oxalyl chloride (11.0 mL, 130 mmol) is added and the reaction mixture heated to reflux for a period of 18 h. Subsequently the solvent is removed in vacuo and the remaining solid is washed twice with 20 mL portions of diethyl ether. The resulting chloroformamidinium chloride is dissolved in acetonitrile (30 mL). This solution is added to a suspension of *N,N*-dimethyl-*p*-phenylenediamine-dihydrochloride (4.38 g, 21 mmol) and triethylamine (13 mL, 93 mmol) in acetonitrile (45 mL) at -5 °C. Then the reaction mixture is stirred for 3 h at 0 °C and additional 2 h at room temperature. The solvent is removed in vacuo and the solid residue dissolved in aqueous HCl (5 %). After addition of aqueous NaOH (40 %) the resulting mixture is extracted with diethyl ether. The organic phases are dried with K<sub>2</sub>CO<sub>3</sub> and the solvent is removed in vacuo. The residual oil is purified by distillation under vacuum. Compound **5a** is obtained as a pale-yellow oil (4.3 g, 18 mmol) in a yield of 87 %. <sup>1</sup>H NMR (199.87 MHz, CD<sub>3</sub>CN, 25 °C): δ = 6.69–6.64 (m, 2 H, CH<sub>arom.</sub>), 6.53–6.49 (m, 2 H, CH<sub>arom.</sub>), 2.80 (s, 6 H, CH<sub>3</sub>), 2.61 ppm (s, 24 H, CH<sub>3</sub>); <sup>13</sup>C NMR (100.56 MHz, 296 K, CD<sub>3</sub>CN): δ = 41.4 (CH<sub>3</sub>), 114.7 (CH<sub>arom.</sub>), 122.5 (CH<sub>arom.</sub>), 143.6 (C<sub>q</sub>), 145.8 (C<sub>q</sub>), 159.0 (C<sub>q</sub>) ppm; ESI<sup>+</sup>: *m/z* = 234.9722 [MH<sup>+</sup>]; elemental analysis (%) for  $C_{13}H_{22}N_4$  (234.34 g mol<sup>-1</sup>): calcd. C 66.63, H 9.46, N 23.91; found C 66.11, H 9.88, N 24.24.

***N,N'*-Dimethylethyleneguanidino-*N''*,*N'''*-dimethyl-*p*-phenylenediamine (5b)**: Oxalyl chloride (6.5 mL, 82 mmol) is added to a solution of 1,3-imidazole-2-imidazolidinone (1.75 mL, 15 mmol) in chloroform (25 mL). Then the reaction mixture is heated to reflux for 18 h. Subsequently the solvent is removed in vacuo and the solid residue washed twice with 20 mL portions of diethyl ether. The resulting chloroformamidinium-chloride is dissolved in acetonitrile (20 mL). This solution is added to a suspension of *N,N*-dimethyl-*p*-phenylenediamine-dihydrochloride (2.53 g, 12 mmol) and triethylamine (7.5 mL, 54 mmol) in acetonitrile (35 mL) at -5 °C, and the reaction mixture is stirred for 3 h at 0 °C and additional 2 h at room temperature. The solvent is removed in vacuo and the solid residue dissolved in aqueous HCl (5 %). Then aqueous NaOH (40 %) is added and the resulting mixture extracted with diethyl ether. The organic phases are dried with K<sub>2</sub>CO<sub>3</sub> and the solvent is removed in vacuo. For further purification, the solid residue is re-dissolved in diethyl ether and precipitated with *n*-hexane. Compound **5b** is obtained as a beige solid (1.52 g, 6.54 mmol) in 55 % yield. Crystals suitable for structural characterization by single-crystal X-ray diffraction were obtained by layering a diethyl ether solution with *n*-hexane. <sup>1</sup>H NMR (199.87 MHz, CD<sub>3</sub>CN, 25 °C): δ = 6.64 (m, 4 H, CH<sub>arom.</sub>), 3.19 (s, 4 H, CH<sub>2</sub>), 2.81 (s, 6 H, CH<sub>3</sub>), 2.53 ppm (s, 6 H, CH<sub>3</sub>); <sup>13</sup>C NMR

(100.56 MHz, 296 K, CD<sub>3</sub>CN): δ = 35.3 (CH<sub>3</sub>), 41.4 (CH<sub>3</sub>), 48.9 (CH<sub>2</sub>), 114.5 (CH<sub>arom.</sub>), 123.1 (CH<sub>arom.</sub>), 141.7 (C<sub>q</sub>), 146.0 (C<sub>q</sub>), 155.8 (C<sub>q</sub>) ppm; elemental analysis (%) for  $C_{13}H_{20}N_4$  (232.33 g mol<sup>-1</sup>): calcd. C 67.21, H 8.68, N 24.11; found C 67.30, H 8.27, N 24.66.

**1,4-Bis(tetramethylguanidino)anthraquinone (6)**: *N,N,N',N''*-Tetramethyl urea (3.0 mL, 25 mmol) is dissolved in CHCl<sub>3</sub> (30 mL) and oxalyl chloride (10.3 mL, 120 mmol) is added. Subsequently the reaction mixture is heated to reflux for 17 h. Then the solvent is removed in vacuo and the remaining solid powder washed twice with 20 mL portions of diethyl ether. The resulting chloroformamidinium-chloride is re-dissolved in CH<sub>3</sub>CN (25 mL). This solution is added to a solution of 1,4-diaminoanthraquinone (2.40 g, 10 mmol) and trimethylamine (7.0 mL, 50 mmol) in CH<sub>3</sub>CN (30 mL) at -5 °C. The reaction mixture is stirred for 2 h at 0 °C and additional 42 h at room temperature. The solvent is removed in vacuo and the remaining solid is re-dissolved in aqueous HCl (5 %). Then aqueous KOH (50 %) is added, and the resulting mixture extracted with diethyl ether. The combined organic phases are washed with brine and dried with K<sub>2</sub>CO<sub>3</sub> and the solvent is removed in vacuo. The solid residue is re-dissolved in CH<sub>3</sub>CN and precipitated by addition of *n*-hexane. 1,4-Bis(tetramethylguanidino)anthraquinone (**6**) is obtained as a red-purple solid (2.7 g, 2.6 mmol) in 62 % yield. Crystals suitable for structural characterization by single-crystal X-ray diffraction are obtained by diffusion of *n*-hexane into a CH<sub>3</sub>CN solution. <sup>1</sup>H NMR (199.87 MHz, CD<sub>3</sub>CN, 25 °C): δ = 8.01–8.06 (m, 2 H, CH<sub>arom.</sub>), 7.65–7.70 (m, 2 H, CH<sub>arom.</sub>), 6.86 (s, 2 H, CH<sub>arom.</sub>), 2.66 ppm (s, 24 H, CH<sub>3</sub>); <sup>13</sup>C NMR (100.56 MHz, 296 K, CD<sub>3</sub>CN): δ = 39.3 (CH<sub>3</sub>), 122.3 (C<sub>q</sub>), 126.2 (CH<sub>arom.</sub>), 133.0 (CH<sub>arom.</sub>), 133.3 (CH<sub>arom.</sub>), 135.8 (C<sub>q</sub>), 149.5 (C<sub>q</sub>), 160.3 (C<sub>q</sub>), 184.2 (C<sub>q</sub>) ppm; IR (KBr):  $\tilde{\nu}$  = 3298 (w), 3084 (w), 3065 (w), 3044 (w), 2994 (w), 2936 (w), 2884 (w), 2803 (w), 1892 (w), 1659 (w), 1611 (w), 1503 (w), 1466 (w), 1443 (w), 1429 (w), 1418 (w), 1404 (w), 1375 (w), 1352 (w), 1325 (m), 1273 (m), 1240 (m), 1188 (m), 1165 (m), 1140 (m), 1111 (w), 1064 (s), 1028 (s), 1015 (m), 966 (w), 943 (s), 924 (s), 897 (m), 866 (s), 841 (s), 831 (w), 799 (s), 775 (w), 752 (m), 741 (m), 729 (vs), 719 (s), 691 (s), 664 (w), 654 (w), 637 (m), 610 (w), 571 (m), 548 (w), 534 (m), 500 (w), 480 (w), 457 (w), 438 (m), 419 (w) cm<sup>-1</sup>; UV/Vis (CH<sub>3</sub>CN, c = 2.0 × 10<sup>-5</sup> mol L<sup>-1</sup>): λ<sub>max</sub> (ε in L mol<sup>-1</sup> cm<sup>-1</sup>) = 544 (4279), 360 (5456), 254 nm (34721) nm; elemental analysis (%) for  $C_{24}H_{30}N_6O_2$  (434.52 g mol<sup>-1</sup>): calcd. C 66.34, H 6.96, N 19.34; found C 66.05, H 6.93, N 19.49.

**(6+2H)(PF<sub>6</sub>)<sub>2</sub>**: A solution of ammonium hexafluorophosphate (0.164 g, 0.89 mmol) in CH<sub>3</sub>CN (10 mL) is prepared. This solution is added to another solution of 1,4-bis[(tetramethyl)guanidino]anthraquinone (0.195 g, 0.448 mmol) in CH<sub>3</sub>CN at room temperature. The reaction mixture is heated to 50 °C and stirred at this temperature for 1 h. Then the mixture is cooled back to room temperature and the solvent removed in vacuo. The solid residue is re-dissolved in CH<sub>3</sub>CN (5 mL) and some charcoal added. Then the mixture is filtered through celite. The obtained solution is layered with diethyl ether. One obtains **(6+2H)(PF<sub>6</sub>)<sub>2</sub>** as orange crystals (0.326 g, 0.448 mmol) in quantitative yield. The crystals are suitable for structural characterization by single-crystal X-ray diffraction. <sup>1</sup>H NMR (199.87 MHz, CD<sub>3</sub>CN, 25 °C): δ = 10.96 (s, 2 H, NH), 8.23–8.28 (m, 2 H, CH<sub>arom.</sub>), 7.89–7.94 (m, 2 H, CH<sub>arom.</sub>), 7.32 (s, 2 H, CH<sub>arom.</sub>), 3.05 ppm (s, 24 H, CH<sub>3</sub>); <sup>13</sup>C NMR (100.56 MHz, 296 K, CD<sub>3</sub>CN): δ = 40.8 (CH<sub>3</sub>), 119.0 (C<sub>q</sub>), 127.6 (CH<sub>arom.</sub>), 127.8 (CH<sub>arom.</sub>), 133.7 (C<sub>q</sub>), 135.9 (CH<sub>arom.</sub>), 137.6 (C<sub>q</sub>), 158.1 (C<sub>q</sub>), 186.9 (C<sub>q</sub>); IR (KBr):  $\tilde{\nu}$  = 3464 (w), 2963 (w), 2926 (w), 2818 (w), 1632 (m), 1595 (w), 1587 (w), 1543 (m), 1501 (w), 1476 (w), 1431 (m), 1415 (m), 1350 (m), 1298 (w), 1263 (s), 1225 (w), 1180 (m), 1172 (m), 1115 (w), 1074 (s), 1047 (w), 1038 (w), 1018 (w), 986 (w), 947 (w), 833 (vs), 781 (w), 735 (s), 704 (w), 685 (w), 669 (w), 664 (w), 625 (w), 557 (vs), 503 (w), 494 (w), 444 (w), 419 (w) cm<sup>-1</sup>; UV/Vis (CH<sub>3</sub>CN, c = 3.28 × 10<sup>-5</sup> mol L<sup>-1</sup>): λ<sub>max</sub> (ε in L mol<sup>-1</sup> cm<sup>-1</sup>) = 456

(5040), 321 (9855), 257 (37747) nm; elemental analysis (%) for  $C_{24}H_{32}N_6O_2P_2F_{12}$  (726.47 g mol<sup>-1</sup>): calcd. C 39.68, H 4.44, N 11.57; found C 39.72, H 5.23, N 11.43.

**1,4-Bis(*N,N'*-dimethylethylenguanidino)anthraquinone (7):** A solution of 1,3-imidazol-2-imidazolidinone (2.7 mL, 25 mmol) in  $CHCl_3$  (30 mL) is prepared and oxalyl chloride (10.6 mL, 125 mmol) is added. The reaction mixture is heated for 20 h under reflux. Subsequently the solvent is removed in vacuo and the residual is washed with diethyl ether and dried under vacuum. The resulting solid product (2-chloro-1,3-dimethyl-4,5-dihydro-1*H*-imidazolium chloride) is dissolved in  $CH_3CN$  and added to a solution of 1,4-diaminoanthraquinone (2.4 g, 10 mmol) and triethylamine (7.0 mL, 50 mmol) in  $CH_3CN$  at -5 °C. After completing the addition, the reaction mixture is stirred for 2 h at 0 °C and additional 18 h at room temperature. Then the solvent is removed under reduced pressure and the remaining solid is re-dissolved in aqueous HCl (5 %). After addition of aqueous NaOH (25 %), the resulting mixture is extracted with ethyl acetate. The combined organic phases are washed with brine, dried with  $K_2CO_3$  and the solvent is removed in vacuo. The residue is dissolved in toluene and precipitated by the addition of *n*-hexane. 1,4-Bis(*N,N'*-dimethylethylenguanidino)anthraquinone (7) is obtained as a red-purple solid (2.88 g, 6.69 mmol) in 67 % yield. <sup>1</sup>H NMR (199.87 MHz,  $CD_3CN$ , 25 °C):  $\delta$  = 8.01–8.09 (m, 2 H,  $CH_{arom.}$ ), 7.66–7.71 (m, 2 H,  $CH_{arom.}$ ), 6.98 (s, 2 H,  $CH_{arom.}$ ), 3.31 (s, 8 H,  $CH_2$ ), 2.58 ppm (s, 12 H,  $CH_3$ ); <sup>13</sup>C NMR (100.56 MHz, 296 K,  $CD_3CN$ ):  $\delta$  = 34.7 ( $CH_3$ ), 48.6 ( $CH_2$ ), 122.1 ( $C_q$ ), 126.2 ( $CH_{arom.}$ ), 132.9 ( $CH_{arom.}$ ), 133.3 ( $CH_{arom.}$ ), 135.6 ( $C_q$ ), 147.7 ( $C_q$ ), 156.5 ( $C_q$ ), 183.4 ( $C_q$ ) ppm; IR (KBr):  $\tilde{\nu}$  = 2948 (w), 2852 (w), 1992 (w), 1995 (w), 1657 (m), 1599 (m), 1537 (w), 1493 (m), 1457 (w), 1441 (w), 1420 (m), 1396 (m), 1368 (w), 1352 (s), 1287 (s), 1243 (m), 1218 (m), 1197 (w), 1167 (m), 1160 (s), 1147 (s), 1117 (w), 1093 (w), 1077 (m), 1059 (vs), 1039 (vs), 1032 (vs), 1024 (s), 987 (s), 980 (s), 968 (m), 943 (s), 904 (m), 892 (w), 878 (s), 853 (s), 800 (s), 766 (m), 760 (m), 729 (vs), 702 (w), 691 (w), 674 (m), 660 (m), 648 (m), 636 (m), 610 (m), 602 (m), 577 (m), 543 (s), 507 (w), 490 (w), 475 (s), 443 (w), 416 (w)  $cm^{-1}$ ; UV/Vis ( $CH_3CN$ ,  $c = 3.26 \times 10^{-5}$  mol L<sup>-1</sup>):  $\lambda_{max}$  ( $\epsilon$  in L mol<sup>-1</sup>  $cm^{-1}$ ) = 536 (4933), 349 (5494), 252 (42250) nm; elemental analysis (%) for  $C_{24}H_{26}N_6O_2$  (430.45 g mol<sup>-1</sup>): calcd. C 66.95, H 6.06, N 19.52; found C 66.81, H 5.94, N 19.32.

**(7+2H)(PF<sub>6</sub>)<sub>2</sub>:** A solution of ammonium hexafluorophosphate (63 mg, 0.39 mmol) in  $CH_3CN$  (8 mL) is added to a solution of 1,4-bis(*N,N'*-dimethylethylenguanidino)anthraquinone (7, 90 mg, 0.21 mmol) in  $CH_3CN$  (8 mL). The reaction mixture is stirred for 2 h at 50 °C and additional 18 h at room temperature. The solvent is removed in vacuo and the solid residue is re-dissolved in  $CH_3CN$  (5 mL). After addition of charcoal the solution is filtered through celite. Half of the solvent is removed and the solution layered with diethyl ether. One obtains (7+2H)(PF<sub>6</sub>)<sub>2</sub> (0.144 g, 0.199 mmol) as orange crystals in 97 % yield. <sup>1</sup>H NMR (199.87 MHz,  $CD_3CN$ , 25 °C):  $\delta$  = 11.32 (s, 2 H, NH), 8.29–8.344 (m, 2 H,  $CH_{arom.}$ ), 7.94–7.99 (m, 2 H,  $CH_{arom.}$ ), 7.47 (s, 2 H,  $CH_{arom.}$ ), 3.88 (s, 8 H,  $CH_2$ ), 2.95 ppm (s, 12 H,  $CH_3$ ); <sup>13</sup>C NMR (100.56 MHz, 296 K  $CD_3CN$ ):  $\delta$  = 34.8 ( $CH_3$ ), 49.3 ( $CH_2$ ), 119.0 ( $C_q$ ), 127.6 ( $CH_{arom.}$ ), 127.8 ( $CH_{arom.}$ ), 133.7 ( $C_q$ ), 136.0 ( $CH_{arom.}$ ), 137.0 ( $C_q$ ), 156.9 ( $C_q$ ), 187.0 ( $C_q$ ) ppm; IR (KBr):  $\tilde{\nu}$  = 3463 (w), 3167 (w), 3114 (w), 2952 (w), 2903 (w), 1617 (s), 1589 (s), 1578 (s), 1499 (s), 1458 (w), 1429 (m), 1399 (m), 1378 (w), 1343 (m), 1311 (m), 1264 (m), 1233(w), 1191 (w), 1161 (w), 1072 (s), 1035 (m), 1021 (w), 983 (w), 946 (w), 901 (m), 878 (vs), 832 (vs), 804 (m), 734 (vs), 714 (w), 668 (w), 648 (m), 590 (w), 557 (vs), 503 (w), 441 (m), 417 (w)  $cm^{-1}$ ; UV/Vis ( $CH_3CN$ ,  $c = 2.66 \times 10^{-5}$  mol L<sup>-1</sup>):  $\lambda_{max}$  ( $\epsilon$  in L mol<sup>-1</sup>  $cm^{-1}$ ) = 462 (6488), 313 (9503), 255 (51516) nm; elemental analysis (%) for  $C_{24}H_{28}N_6O_2P_2F_{12}$  (722.44 g mol<sup>-1</sup>): calcd. C 39.90, H 3.91, N 11.63; found C 40.80, H 4.25, N 13.04.

**1,5-Bisguanidinonaphthalene Dihydrochloride (8·2HCl):** A 2 M solution of HCl in diethyl ether (6.5 mL, 13 mmol) is added to a suspension of 1,5-diamino-naphthalene (1.00 g, 6.35 mmol) in 50 mL of diethyl ether. The reaction mixture is stirred overnight at room temperature. After solvent removal under vacuum the crude product is re-dissolved in 100 mL of ethanol. Cyanamide (1.556 g, 44.0 mmol) is added and the solution is heated to reflux overnight. The volume of the resulting dark purple solution is reduced under vacuo to a minimum. Diethyl ether is added and the precipitate filtered. The residue is washed with diethyl ether and dried under vacuo to give 1,5-bisguanidinonaphthalene-dihydrochloride, 8·2HCl, as a light-grey solid (1.85 g, 5.9 mmol) in 93 % yield. Crystals suitable for structural characterization by single-crystal X-ray diffraction are obtained by layering a methanol solution with diethyl ether. Elemental analysis (%) for  $C_{12}H_{16}N_6Cl_2$  (315.20 g mol<sup>-1</sup>): calcd. C 45.73, H 5.12, N 26.66; found C 45.24, H 5.43, N 26.07.

**1,5-Bis(tetramethylguanidino)naphthalene (9):** Oxalyl chloride (10.3 mL, 120 mmol) is added to a solution of *N,N,N',N'*-tetramethylurea (3.0 mL, 25 mmol) in chloroform (30 mL). Then the reaction mixture is heated to reflux for 18 h. The solvent is removed in vacuo and the remaining solid washed twice with 20 mL portions of diethyl ether. The resulting chloroformamidinium chloride is dissolved in acetonitrile (25 mL), and this solution added to a suspension of 1,5-diaminonaphthalene (1.58 g, 10 mmol) and triethylamine (7.0 mL, 50 mmol) in acetonitrile (30 mL) at a temperature of -5 °C. Subsequently the reaction mixture is stirred for 3 h at 0 °C and additional 2 h at room temperature. The solvent is removed in vacuo and the solid residue dissolved in aqueous HCl (5 %). Aqueous NaOH (40 %) is added, and the resulting mixture extracted with dichloromethane. The organic phases are dried with  $K_2CO_3$  and the solvent is removed in vacuo. The solid residue is washed with toluene and dried under vacuo to give 1,5-bis(tetramethylguanidino)naphthalene (9) is obtained as a pale-rosy solid (2.7 g, 7.6 mmol) in a yield of 76 %. Crystals suitable for single-crystal X-ray diffraction could be obtained from a solution in *n*-hexane. <sup>1</sup>H NMR (200.13 MHz,  $CD_3CN$ , 25 °C):  $\delta$  = 7.52–7.57 (m, 2 H,  $CH_{arom.}$ ), 7.16–7.23 (m, 2 H,  $CH_{arom.}$ ), 6.44–6.48 (m, 2 H,  $CH_{arom.}$ ), 2.64 ppm (s, 24 H,  $CH_3$ ); <sup>13</sup>C NMR (100.56 MHz, 296 K,  $CD_3CN$ ):  $\delta$  = 39.4 ( $CH_3$ ) ppm. The poor solubility prohibited the detection of more signals; UV/Vis ( $CH_3CN$ ,  $c = 5.53 \times 10^{-5}$  mol L<sup>-1</sup>):  $\lambda_{max}$  ( $\epsilon$  in L mol<sup>-1</sup>  $cm^{-1}$ ) = 345 (17463), 239 nm (40240); elemental analysis (%) for  $C_{20}H_{30}N_6$  (354.49 g mol<sup>-1</sup>): calcd. C 67.76, H 8.53, N 23.71; found C 66.87, H 8.32, N 23.34.

**(9+2H)(PF<sub>6</sub>)<sub>2</sub>:** A solution of ammonium hexafluorophosphate (33 mg, 0.2 mmol) in  $CH_3CN$  (2 mL) is added to a solution of 1,5-bis(tetramethylguanidino)naphthalene (9, 35 mg, 0.10 mmol) in  $CH_3CN$  (7 mL). The reaction mixture is stirred for 1 h at 50 °C and additional 18 h at room temperature. The solvent is removed in vacuo and the solid residue re-dissolved in  $CH_3CN$  (3 mL). After addition of charcoal the solution is filtered through celite. Half of the solvent is removed and the solution layered with diethyl ether. From this solution, one obtains (6+2H)(PF<sub>6</sub>)<sub>2</sub> as colorless crystals, that are structurally characterized by single-crystal X-ray diffraction. Further analysis is not made.

**1,5-Bis(*N,N'*-dimethylethylenguanidino)naphthalene (10):** Oxalyl chloride (5.3 mL, 62.5 mmol) is added to a solution of 1,3-imidazol-2-imidazolidinone (1.35 mL, 12.5 mmol) in chloroform (30 mL). The reaction mixture is heated for 20 h under reflux. Subsequently the solvent is removed in vacuo and the residue washed with diethyl ether and dried under vacuum. The obtained solid is dissolved in acetonitrile (12 mL) and added to a solution of 1,5-diamino-naphthalene (0.774 g, 4.9 mmol) and triethylamine (3.5 mL, 25 mmol) in

acetonitrile at  $-5\text{ }^{\circ}\text{C}$ . The reaction mixture is stirred for 2 h at  $0\text{ }^{\circ}\text{C}$  and another 18 h at room temperature. Then the solvent is removed under reduced pressure and the remaining solid is dissolved in aqueous HCl (5 %). Aqueous NaOH (40 %) is added and the resulting mixture extracted with toluene. The combined organic phases are dried with  $\text{K}_2\text{CO}_3$  and the solvent is removed in vacuo. Finally, the residue is washed with toluene and dried under vacuum. The product 1,5-bis(*N,N'*-dimethylethyleneguanidino)-naphthalene (**10**) is obtained as a pale-pink solid (1.50 g, 4.28 mmol) in 87 % yield. Crystals suitable for structural characterization by single-crystal X-ray diffraction are grown from hot acetonitrile solutions.  $^1\text{H}$  NMR (199.87 MHz,  $\text{CD}_3\text{CN}$ ,  $25\text{ }^{\circ}\text{C}$ ):  $\delta = 7.49\text{--}7.53$  (m, 2 H,  $\text{CH}_{\text{arom}}$ ),  $7.16\text{--}7.23$  (m, 2 H,  $\text{CH}_{\text{arom}}$ ),  $6.74\text{--}6.70$  (m, 2 H,  $\text{CH}_{\text{arom}}$ ),  $2.50$  (s, 8 H,  $\text{CH}_2$ ),  $3.25$  ppm (s, 12 H,  $\text{CH}_3$ );  $^{13}\text{C}$  NMR (100.56 MHz, 296 K,  $\text{CD}_3\text{CN}$ ):  $\delta = 34.7$  ( $\text{CH}_2$ ),  $48.8$  ( $\text{CH}_3$ ) ppm. The poor solubility prohibited the detection of more signals; UV/Vis ( $\text{CH}_3\text{CN}$ ,  $c = 5.31 \times 10^{-5}\text{ mol L}^{-1}$ ):  $\lambda_{\text{max}}$  ( $\epsilon$  in  $\text{L mol}^{-1}\text{ cm}^{-1}$ ) =  $342$  (17933),  $238$  nm (40807); elemental analysis (%) for  $\text{C}_{20}\text{H}_{26}\text{N}_6$  ( $350.46\text{ g mol}^{-1}$ ): calcd. C 68.54, H 7.48, N 23.98; found C 68.55, H 7.21, N 23.48.

### X-ray Crystal Structure Determinations

Crystal data and details of the structure determinations are compiled in a table in the SI. Full shells of intensity data were collected at low temperature with an Enraf Nonius Kappa CCD diffractometer [Mo- $K\alpha$  radiation, sealed X-ray tube, graphite monochromator, compounds **3**·2HCl, **4**·2HCl, **6**, (**7**+2H)( $\text{PF}_6$ )<sub>2</sub>, **8**·2HCl, **9**, (**9**+2H)( $\text{PF}_6$ )<sub>2</sub>, **10**], a Bruker D8 Venture, dual source (Mo- or Cu- $K\alpha$  radiation, microfocus X-ray tube, Photon III Detector, compound **5b**) or with an Agilent Technologies Supernova-E CCD diffractometer [Mo- or Cu- $K\alpha$  radiation, microfocus X-ray tube, multilayer mirror optics, compounds (**3**+2H) $\text{Pb}_2\text{I}_6$ , (**4**+2H) $\text{PbI}_4$ , (**6**+2H)( $\text{PF}_6$ )<sub>2</sub>]. Detector frames (typically w-, occasionally j-scans, scan width  $0.4\text{--}0.1^\circ$ ) were integrated by profile fitting.<sup>[61,62]</sup> Data were corrected for air and detector absorption, Lorentz and polarization effects<sup>[62]</sup> and scaled essentially by application of appropriate spherical harmonic functions.<sup>[62–64]</sup> Absorption by the crystal was treated with a semiempirical multiscan method (as part of the scaling process) and augmented by a spherical correction,<sup>[62,63,64]</sup> or numerically (Gaussian grid).<sup>[62,64,65]</sup> For datasets collected with the microfocus tubes an illumination correction was performed as part of the numerical absorption correction.<sup>[64]</sup>

The structures were solved by ab initio dual space methods involving difference Fourier syntheses (VLD procedure),<sup>[66]</sup> by the heavy atom method combined with structure expansion by direct methods applied to difference structure factors<sup>[67]</sup> or by the charge flip procedure<sup>[68]</sup> and refined by full-matrix least-squares methods based on  $F^2$  against all unique reflections.<sup>[69]</sup> All non-hydrogen atoms were given anisotropic displacement parameters. Hydrogen atoms bound to carbon were input at calculated positions and refined with a riding model. Hydrogen atoms bound to nitrogen were located in difference Fourier syntheses and refined, either fully or with appropriate distance and/or symmetry restraints (variable geometry rigid groups with local  $\text{C}_{3v}$  symmetry for  $[\text{NH}_3]^+$ ). P–F and F...F distances within the  $[\text{PF}_6]^-$  anions were restrained to sensible values during refinement.<sup>[70]</sup> Suitable adp restraints were applied.<sup>[71]</sup>

Due to severe disorder and fractional occupancy, electron density attributed to solvent of crystallization (acetonitrile and *n*-hexane) was removed from the structure of (**6**+2H)( $\text{PF}_6$ )<sub>2</sub> with the BYPASS procedure,<sup>[72]</sup> as implemented in PLATON (squeeze/hybrid).<sup>[73]</sup> Partial structure factors from the solvent masks were included in the refinement as separate contributions to  $F_{\text{calc}}$ .

CCDC 1938180 (for **3**·HCl), 1938184 {for [(**3**+2H) $\text{Pb}_2\text{I}_6$ ]}, 1938181 (for **4**·2HCl), 1938185 {for [(**4**+2H) $\text{PbI}_4$ ]}, 1938183 (for **5b**), 1938175 (for **6**), 1938186 {for [(**6**+2H)( $\text{PF}_6$ )<sub>2</sub>]}, 1938178 {for [(**7**+2H)( $\text{PF}_6$ )<sub>2</sub>]}, 1938176 {for [(**8**+2H) $\text{Cl}_2$ ]}, 1938174 (for **9**), 1938182 {for [(**9**+2H)( $\text{PF}_6$ )<sub>2</sub>]}, 1938177 (for **10**), and 1938179 (for *p*-nitro-tetramethylguanidinobenzene) contain the supplementary crystallographic data for this paper. These data can be obtained free of charge from The Cambridge Crystallographic Data Centre.

### Details of the Quantum Chemical Calculations

Density functional calculations are performed with the program TURBOMOLE.<sup>[74,75,76]</sup> The B3LYP functional<sup>[77,78]</sup> is used with the def2-TZVP or def2-SV(P) basis sets.<sup>[79]</sup> For the calculation of the two-electron integrals, the resolution-of-the-identity (RI) approximation<sup>[80]</sup> is used with the appropriate def2-TZVP or def2-SV(P) auxiliary basis sets.<sup>[81]</sup> To confirm that the optimized structures are minima of the potential energy surfaces and to obtain zero point vibrational energy contributions, vibrational frequencies are calculated. All electronic energies are obtained with the def2-TZVP basis set. For the anthraquinone derivatives, the calculations of the vibrational frequencies relied on the smaller def2-SV(P) basis set. Electronic excitation energies are obtained by time-dependent density functional calculations.<sup>[82,83]</sup> The time-dependent density functional calculations considers the influence of the environment by the conductor-like screening model (COSMO)<sup>[84]</sup> with a value for  $\epsilon_r$  of 38.8 (corresponding to  $\text{CH}_3\text{CN}$ ).

### Acknowledgments

The authors gratefully acknowledge financial support by the BMBF (Perosol project) and the Deutsche Forschungsgemeinschaft (DFG).

**Keywords:** Guanidine ligands · Perovskites · Lead iodide · Electron donors · Redox chemistry

- [1] T. Nishinaga (Ed.), *Organic Redox Systems, Synthesis, Properties and Applications*, John Wiley & Sons, Inc. **2016**.
- [2] J. Broggi, T. Terme, P. Vanelle, *Angew. Chem. Int. Ed.* **2014**, *53*, 384–413; *Angew. Chem.* **2014**, *126*, 392–423.
- [3] a) S. Zhou, H. Farwaha, J. A. Murphy, *Chimia* **2012**, *66*, 418–424; b) J. A. Murphy, *J. Org. Chem.* **2014**, *79*, 3731–3746; c) E. Doni, J. A. Murphy, *Chem. Commun.* **2014**, *50*, 6073–6087.
- [4] J. Hankache, O. S. Wenger, *Chem. Rev.* **2011**, *111*, 5138–5178.
- [5] H.-J. Himmel, *Synlett* **2018**, *29*, 1957–1977.
- [6] a) B. Eberle, O. Hübner, A. Ziesak, E. Kaifer, H.-J. Himmel, *Chem. Eur. J.* **2015**, *21*, 8578–8590; b) H.-J. Himmel, *Z. Anorg. Allg. Chem.* **2013**, *639*, 1940–1952.
- [7] J. Hornung, O. Hübner, E. Kaifer, H.-J. Himmel, *RSC Adv.* **2016**, *6*, 39323–39329.
- [8] A. Peters, E. Kaifer, H.-J. Himmel, *Eur. J. Org. Chem.* **2008**, 5907–5914.
- [9] B. Eberle, E. Kaifer, H.-J. Himmel, *Angew. Chem. Int. Ed.* **2017**, *56*, 3360–3363; *Angew. Chem.* **2017**, *129*, 3408–3412.
- [10] U. Wild, S. Federle, A. Wagner, E. Kaifer, H.-J. Himmel, *Chem. Eur. J.* **2016**, *22*, 11971–11976.
- [11] U. Wild, F. Schön, H.-J. Himmel, *Angew. Chem. Int. Ed.* **2017**, *56*, 16410–16413; *Angew. Chem.* **2017**, *129*, 16630–16633.
- [12] For some review articles about proton-coupled electron transfer reactions, see: a) S. J. Slattery, J. K. Blahö, J. Lehn, K. A. Goldsby, *Coord. Chem. Rev.* **1998**, *174*, 391–416; b) C. Costentin, M. Robert, J.-M. Savéant, *Chem. Rev.* **2008**, *108*, 2145–2179; c) J. J. Consepacion, J. W. Jurss, M. K. Brennaman, P. G. Hoertz, A. O. T. Patrocínio, N. Y. M. Iha, J. L. Templeton, T. J. Meyer, *Acc. Chem. Res.* **2009**, *42*, 1954–1965; d) S. Y. Reece, D. G. Nocera, *Annu. Rev. Biochem.* **2009**, *78*, 673–699; e) J. J. Warren, T. A. Tronic, J. M. Mayer, *Chem. Rev.* **2010**, *110*, 6961–7001; f) S. Hammes-

- Schiffer, A. A. Stuchebrukhov, *Chem. Rev.* **2010**, *110*, 6939–6960; g) S. Hammes-Schiffer, *J. Am. Chem. Soc.* **2015**, *137*, 8860–8871; h) I. Siewert, *Chem. Eur. J.* **2015**, *21*, 15078–15091; i) D. C. Miller, K. T. Tarantino, R. R. Knowles, *Top. Curr. Chem. (Z)* **2016**, *374*:30; j) E. C. Gentry, R. R. Knowles, *Acc. Chem. Res.* **2016**, *49*, 1546–1556; k) J. C. Lennox, D. A. Kurtz, T. Huang, J. L. Dempsey, *ACS Energy Lett.* **2017**, *2*, 1246–1256; l) A. Pannwitz, O. S. Wenger, *Dalton Trans.* **2019**, *48*, 5861–5868.
- [13] See, for example: I. Kaljurand, A. Kütt, L. Sooväli, T. Rodima, V. Mäemets, I. Leito, I. A. Koppel, *J. Org. Chem.* **2005**, *70*, 1019–1028.
- [14] T. Ishikawa (Ed.), *Superbases for Organic Synthesis*, John Wiley & Sons, Ltd. **2009**.
- [15] H. Bredereck, K. Bredereck, *Chem. Ber.* **1961**, *94*, 2278–2295.
- [16] U. Wild, O. Hübner, L. Greb, M. Enders, E. Kaifer, H.-J. Himmel, *Eur. J. Org. Chem.* **2018**, 5910–5915.
- [17] H. Herrmann, P. Walter, E. Kaifer, H.-J. Himmel, *Eur. J. Inorg. Chem.* **2017**, 5539–5544.
- [18] a) B. V. Lotsch, *Angew. Chem. Int. Ed.* **2014**, *53*, 635–637; *Angew. Chem.* **2014**, *126*, 647–649; b) P. Gao, M. Grätzel, M. K. Nazeeruddin, *Energy Environ. Sci.* **2014**, *7*, 2448–2463; c) C. C. Stoumpos, M. G. Kanatzidis, *Acc. Chem. Res.* **2015**, *48*, 2791–2802; d) A. Senocrate, J. Maier, *J. Am. Chem. Soc.* **2019**, *141*, 8382–8396.
- [19] Z. Wang, Z. Shi, T. Li, Y. Chen, W. Huang, *Angew. Chem. Int. Ed.* **2017**, *56*, 1190–1212; *Angew. Chem.* **2017**, *129*, 1210–1233.
- [20] a) M. M. Lee, J. Teuscher, T. Miyasaka, T. N. Murakami, H. J. Snaith, *Science* **2012**, *338*, 643–647; b) M. Liu, M. B. Johnston, H. J. Snaith, *Nature* **2013**, *501*, 395–398.
- [21] Z. Zhao, F. Gu, H. Rao, S. Ye, Z. Liu, Z. Bian, C. Huang, *Adv. Energy Mater.* **2019**, *9*, 1802671 (1–28).
- [22] X. Zhang, L. Li, Z. Sun, J. Luo, *Chem. Soc. Rev.* **2019**, *48*, 517–539.
- [23] D. Weber, *Z. Naturforsch. B* **1978**, *33*, 1443–1445.
- [24] a) M. Szafranski, *Thermochim. Acta* **1997**, *307*, 177–183; b) N. De Marco, H. Zhou, Q. Chen, P. Sun, Z. Liu, L. Meng, E.-P. Yao, Y. Liu, A. Schiffer, Y. Yang, *Nano Lett.* **2016**, *16*, 1009–1016; c) L. Dimesso, A. Quintilla, Y.-M. Kim, U. Lemmer, W. Jaegermann, *Mater. Sci. Eng. B* **2016**, *204*, 27–33.
- [25] G. Giorgi, J.-I. Fujisawa, H. Segawa, K. Yamashita, *J. Phys. Chem. C* **2015**, *119*, 4694–4701.
- [26] A. D. Jodlowski, A. Yépez, R. Luque, L. Camacho, G. de Miguel, *Angew. Chem. Int. Ed.* **2016**, *55*, 14972–14977; *Angew. Chem.* **2016**, *128*, 15196–15201.
- [27] M. Wilke, N. Casati, *Chem. Eur. J.* **2018**, *24*, 17701–17711.
- [28] N. Pellet, P. Gao, G. Gregori, T.-Y. Yang, M. K. Nazeeruddin, J. Maier, M. Grätzel, *Angew. Chem. Int. Ed.* **2014**, *53*, 3151–3157; *Angew. Chem.* **2014**, *126*, 3215–3221.
- [29] C. Yi, J. Luo, S. Meloni, A. Boziki, N. Ashari-Astani, C. Grätzel, *Energy Environ. Sci.* **2016**, *9*, 656–662.
- [30] W. Ke, I. Spanopoulos, Q. Tu, I. Hadar, X. Li, G. S. Shekhawat, V. P. Dravid, M. G. Kanatzidis, *J. Am. Chem. Soc.* **2019**, *141*, 8627–8637.
- [31] D. B. Mitzi, *J. Chem. Soc., Dalton Trans.* **2001**, 1–12.
- [32] Y. Zhang, J. Liu, Z. Wang, Y. Xue, Q. Ou, L. Polavarapu, J. Zheng, X. Qi, Q. Bao, *Chem. Commun.* **2016**, *52*, 13637–13655.
- [33] L. Mao, C. C. Stoumpos, M. G. Kanatzidis, *J. Am. Chem. Soc.* **2019**, *141*, 1171–1190.
- [34] M. Safdari, P. H. Svensson, M. T. Hoang, I. Oh, L. Kloo, J. M. Gardner, *J. Mater. Chem. A* **2016**, *4*, 15638–15646.
- [35] a) D. B. Mitzi, C. A. Feild, W. T. A. Harrison, A. M. Guloy, *Nature* **1994**, *369*, 467–469; b) C. C. Stoumpos, D. H. Cao, D. J. Clark, J. Young, J. M. Rondinelli, J. I. Jang, J. T. Hupp, M. G. Kanatzidis, *Chem. Mater.* **2016**, *28*, 2852–2867; c) D. H. Cao, C. C. Stoumpos, O. K. Farha, J. T. Hupp, M. G. Kanatzidis, *J. Am. Chem. Soc.* **2015**, *137*, 7843–7850.
- [36] A. Mei, X. Li, L. Liu, Z. Ku, T. Liu, Y. Rong, M. Xu, M. Hu, J. Chen, Y. Yang, M. Grätzel, H. Han, *Science* **2014**, *345*, 295–298.
- [37] I. C. Smith, E. T. Hoke, D. Solis-Ibarra, M. D. McGehee, H. I. Karunadasa, *Angew. Chem. Int. Ed.* **2014**, *53*, 11232–11235; *Angew. Chem.* **2014**, *126*, 11414–11417.
- [38] C. C. Boyd, R. Cheacharoen, T. Leijtens, M. D. McGehee, *Chem. Rev.* **2019**, *119*, 3418–3451.
- [39] N. I. Selivanov, A. A. Murashkina, R. Kevorkyants, A. V. Emeline, D. W. Bahnemann, *Dalton Trans.* **2018**, *47*, 16313–16319.
- [40] M. Konstantakou, T. Stergiopoulos, *J. Mater. Chem. A* **2017**, *5*, 11518–11549.
- [41] C. C. Stoumpos, C. D. Malliakas, M. G. Kanatzidis, *Inorg. Chem.* **2013**, *52*, 9019–9038.
- [42] M.-G. Ju, J. Dai, L. Ma, X. C. Zeng, *J. Am. Chem. Soc.* **2017**, *139*, 8038–8043.
- [43] F. Hao, C. C. Stoumpos, D. H. Cao, R. P. H. Chang, M. G. Kanatzidis, *Nat. Photonics* **2014**, *8*, 489–494.
- [44] N. K. Noel, S. D. Stranks, A. Abate, C. Wehrenfennig, S. Guarnera, A.-A. Haghighirad, A. Sadhanala, G. E. Eperon, S. K. Pathak, M. B. Johnston, A. Petrozza, L. M. Herz, H. J. Snaith, *Energy Environ. Sci.* **2014**, *7*, 3061–3068.
- [45] Z. Xiao, W. Meng, J. Wang, D. B. Mitzi, Y. Yan, *Mater. Horiz.* **2017**, *4*, 206–216.
- [46] W. Ke, C. C. Stoumpos, M. G. Kanatzidis, *Adv. Mater.* **2018**, *30*, 1803230 (1–31).
- [47] L. Chung, B. Lee, J. He, R. P. H. Chang, M. G. Kanatzidis, *Nature* **2012**, *485*, 486–489.
- [48] a) M. H. Kumar, S. Dharani, W. L. Leong, P. P. Boix, R. R. Prabhakar, T. Baikie, C. Shi, H. Ding, R. Ramesh, M. Asta, M. Gratezel, S. G. Mhaisalkar, N. Mathews, *Adv. Mater.* **2014**, *26*, 7122–7127; b) S. J. Lee, S. S. Shin, Y. C. Kim, D. Kim, T. K. Ahn, J. H. Noh, J. Seo, S. I. Seok, *J. Am. Chem. Soc.* **2016**, *138*, 3974–3977; c) D. Sabba, H. K. Mulmudi, R. R. Prabhakar, T. Krishnamoorthy, T. Baikie, P. P. Boix, S. Mhaisalkar, N. Mathews, *J. Phys. Chem. C* **2015**, *119*, 1763–1767.
- [49] K. P. Marshall, M. Walker, R. I. Walton, R. A. Hatton, *Nat. Energy* **2016**, *1*, 16178.
- [50] T.-B. Song, T. Yokoyama, C. C. Stoumpos, J. Logsdon, D. H. Cao, M. R. Wasielewski, S. Aramaki, M. G. Kanatzidis, *J. Am. Chem. Soc.* **2017**, *139*, 836–842.
- [51] a) C. Wurster, E. Schobig, *Ber. Dtsch. Chem. Ges.* **1879**, *12*, 1807–1813; b) C. Wurster, *Ber. Dtsch. Chem. Ges.* **1879**, *12*, 2071–2072; c) C. Wurster, *Ber. Dtsch. Chem. Ges.* **1887**, *20*, 808–810.
- [52] a) L. Michaelis, E. S. Hill, *J. Am. Chem. Soc.* **1933**, *55*, 1481–1494; b) L. Michaelis, M. P. Schubig, S. Granick, *J. Am. Chem. Soc.* **1939**, *61*, 1981–1992.
- [53] S. V. Rosokha, J. K. Kochi, *J. Am. Chem. Soc.* **2007**, *129*, 3683–3697.
- [54] I. Antol, Z. Glasovac, D. Margetić, R. Crespo-Otero, M. Barbatti, *J. Phys. Chem. A* **2016**, *120*, 7088–7100.
- [55] M. P. Hautzinger, J. Dai, Y. Ji, Y. Fu, J. Chen, I. A. Guzei, J. Wright, Y. Li, S. Jin, *Inorg. Chem.* **2017**, *56*, 14991–14998.
- [56] For a similar analysis, see for example: A. E. Maughan, J. A. Kurzman, J. R. Neilson, *Inorg. Chem.* **2015**, *54*, 370–378.
- [57] K.-z. Du, Q. Tu, X. Zhang, Q. Han, J. Liu, S. Zauscher, D. B. Mitzi, *Inorg. Chem.* **2017**, *56*, 9291–9302.
- [58] For TG/DSC analysis of  $\text{CH}_3\text{NH}_3\text{Ml}_3$  perovskites (M = Sn or Pb), see the examples given in ref.<sup>[41]</sup>.
- [59] T. Li, W. A. Dunlap-Shohl, Q. Han, D. B. Mitzi, *Chem. Mater.* **2017**, *29*, 6200–6204.
- [60] T. Li, W. A. Dunlap-Shohl, E. W. Reinheimer, P. Le Magueres, D. B. Mitzi, *Chem. Sci.* **2019**, *10*, 1168–1175.
- [61] K. Kabsch, in: M. G. Rossmann, E. Arnold (Eds.), *International Tables for Crystallography Vol. F*, Ch. 11.3, Kluwer Academic Publishers, Dordrecht, The Netherlands, **2001**.
- [62] a) *DENZO-SMN*, Z. Otwinowski & W. Minor, Processing of X-ray Diffraction Data Collected in Oscillation Mode, Methods Enzymol. (1997), p. 276 (Eds.: C. W. Carter, R. M. Sweet), Academic Press; b) *SAINT*, Bruker AXS GmbH, Karlsruhe, Germany **2017**; c) *CrysAlisPro*, Agilent Technologies UK Ltd., Oxford, UK **2011–2014** and Rigaku Oxford Diffraction, Rigaku Polska Sp.z o.o., Wrocław, Poland **2015–2019**.
- [63] R. H. Blessing, *Acta Crystallogr., Sect. A* **1995**, *51*, 33–38.
- [64] a) *SCALE3 ABSPACK*, *CrysAlisPro*, Agilent Technologies UK Ltd., Oxford, UK **2011–2014** and Rigaku Oxford Diffraction, Rigaku Polska Sp.z o.o., Wrocław, Poland **2015–2019**; b) G. M. Sheldrick, *SADABS*, Bruker AXS GmbH, Karlsruhe, Germany **2004–2014**; c) L. Krause, R. Herbst-Irmer, G. M. Sheldrick, D. Stalke, *J. Appl. Crystallogr.* **2015**, *48*, 3–10.
- [65] W. R. Busing, H. A. Levy, *Acta Crystallogr.* **1957**, *10*, 180–182.
- [66] a) M. C. Burla, R. Caliandro, B. Carrozzini, G. L. Cascarano, C. Cuocci, C. Giacovazzo, M. Mallamo, A. Mazzzone, G. Polidori, *SIR2014*, CNR IC, Bari, Italy, **2014**; b) M. C. Burla, R. Caliandro, B. Carrozzini, G. L. Cascarano, C. Cuocci, C. Giacovazzo, M. Mallamo, A. Mazzzone, G. Polidori, *J. Appl. Crystallogr.* **2015**, *48*, 306–309.

- [67] a) P. T. Beurskens, G. Beurskens, R. de Gelder, J. M. M. Smits, S. Garcia-Granda, R. O. Gould, *DIRDIF-2008*, Radboud University Nijmegen, The Netherlands, **2008**; b) P. T. Beurskens, in: G. M. Sheldrick, C. Krüger, R. Goddard (Eds.), *Crystallographic Computing 3*, Clarendon Press, Oxford, UK, **1985**, p. 216.
- [68] a) L. Palatinus, *SUPERFLIP*, EPF Lausanne, Switzerland and Fyzikální ústav AV ČR, v. v. i., Prague, Czech Republic, **2007–2014**; b) L. Palatinus, G. Chapuis, *J. Appl. Crystallogr.* **2007**, *40*, 786–790.
- [69] a) G. M. Sheldrick, *SHELXL-20xx*, University of Göttingen and Bruker AXS GmbH, Karlsruhe, Germany **2012–2018**; b) W. Robinson, G. M. Sheldrick in: N. W. Isaaks, M. R. Taylor (Eds.), *Crystallographic Computing 4*, Ch. 22, IUCr and Oxford University Press, Oxford, UK, **1988**; c) G. M. Sheldrick, *Acta Crystallogr., Sect. A* **2008**, *64*, 112–122; d) G. M. Sheldrick, *Acta Crystallogr., Sect. C* **2015**, *71*, 3–8.
- [70] a) J. S. Rollett in: F. R. Ahmed, S. R. Hall, C. P. Huber (Eds.), *Crystallographic Computing* p. 167, Munksgaard, Copenhagen, Denmark, **1970**; b) D. Watkin in: N. W. Isaaks, M. R. Taylor (Eds.), *Crystallographic Computing 4*, Ch. 8, IUCr and Oxford University Press, Oxford, UK, **1988**; c) P. Müller, R. Herbst-Irmer, A. L. Spek, T. R. Schneider, M. R. Sawaya in: P. Müller (Eds.), *Crystal Structure Refinement*, Ch. 5, Oxford University Press, Oxford, UK, **2006**; d) D. Watkin, *J. Appl. Crystallogr.* **2008**, *41*, 491–522.
- [71] a) J. S. Rollett in: F. R. Ahmed, S. R. Hall, C. P. Huber (Eds.), *Crystallographic Computing* p. 167, Munksgaard, Copenhagen, Denmark, **1970**; b) A. Thorn, B. Dittrich, G. M. Sheldrick, *Acta Crystallogr., Sect. A* **2012**, *68*, 448–451.
- [72] a) P. van der Sluis, A. L. Spek, *Acta Crystallogr., Sect. A* **1990**, *46*, 194–201; b) A. L. Spek, *Acta Crystallogr., Sect. C* **2015**, *71*, 9–18.
- [73] a) A. L. Spek, *PLATON*, Utrecht University, The Netherlands; b) A. L. Spek, *J. Appl. Crystallogr.* **2003**, *36*, 7–13.
- [74] TURBOMOLE V7.2 **2017**, a development of University of Karlsruhe and Forschungszentrum Karlsruhe GmbH, 1989–2007, TURBOMOLE GmbH, since 2007; available from <http://www.turbomole.com>.
- [75] R. Ahlrichs, M. Bär, M. Häser, H. Horn, C. Kölmel, *Chem. Phys. Lett.* **1989**, *162*, 165–169.
- [76] O. Treutler, R. Ahlrichs, *J. Chem. Phys.* **1995**, *102*, 346–354.
- [77] A. D. Becke, *J. Chem. Phys.* **1993**, *98*, 5648–5652.
- [78] P. J. Stephens, F. J. Devlin, C. F. Chabalowski, M. J. Frisch, *J. Phys. Chem.* **1994**, *98*, 11623–11627.
- [79] F. Weigend, R. Ahlrichs, *Phys. Chem. Chem. Phys.* **2005**, *7*, 3297–3305.
- [80] K. Eichkorn, O. Treutler, H. Öhm, M. Häser, R. Ahlrichs, *Chem. Phys. Lett.* **1995**, *242*, 652–660.
- [81] F. Weigend, *Phys. Chem. Chem. Phys.* **2006**, *8*, 1057–1065.
- [82] R. Bauernschmitt, R. Ahlrichs, *Chem. Phys. Lett.* **1996**, *256*, 454–464.
- [83] R. Bauernschmitt, M. Häser, O. Treutler, R. Ahlrichs, *Chem. Phys. Lett.* **1997**, *264*, 573–578.
- [84] A. Klamt, G. Schürmann, *J. Chem. Soc., Perkin Trans. 2* **1993**, 799–805.

---

Received: September 12, 2019